Thermoelectric power and its correlation with conductivity in NbS_3 whiskers

S. G. Zybtsev,[1] V. Ya. Pokrovskii,[1,*] V. F. Nasretdinova,[1,2] S. V. Zaitsev-Zotov,[1] V. V. Pryadun,[3] E. S. Kozlyakova,[3] O. S. Volkova,[3,4,5] A. N. Vasiliev,[3,4,6] Woei Wu Pai,[7,8,†] and D. Starešinić[9]

[1]*Kotel'nikov Institute of Radioengineering and Electronics of RAS, Mokhovaya 11-7, 125009 Moscow, Russia*
[2]*CENN Nanocenter, Jamova 39, 1000 Ljubljana, Slovenia*
[3]*Low Temperature Physics and Superconductivity Department, M. V. Lomonosov Moscow State University, 119991 Moscow, Russia*
[4]*National University of Science and Technology MISiS, 119991 Moscow, Russia*
[5]*Ural Federal University, 620002 Ekaterinburg, Russia*
[6]*National Research South Ural State University, 454080 Chelyabinsk, Russia*
[7]*Center for Condensed Matter Sciences, National Taiwan University, Taipei 106, Taiwan*
[8]*Department of Physics, National Taiwan University, Taipei 106, Taiwan*
[9]*Institute of Physics, Bijenička cesta 46, HR-10000 Zagreb, Croatia*

(Received 19 September 2017; published 27 June 2019)

We report studies of the Seebeck coefficient S of the quasi-one-dimensional compound NbS_3, together with the temperature dependence of its specific conductivity σ_s and heat capacity c_p. The monoclinic phase (NbS_3-II) is studied over the temperature range $T = 80$–400 K, which covers two charge density wave (CDW) transitions at $T_{P1} = 360$ K (CDW-1) and $T_{P2} = 150$ K (CDW-2). The $S(T)$ curves show features in the vicinities of both CDW transitions and appear to be correlated with the value of $\sigma_s(300\ \mathrm{K})$: The increase of S below T_{P1} in the high-Ohmic samples reveals a complete dielectrization of the electronic spectrum, while in the low-Ohmic samples S decreases below T_{P1} and even becomes negative below T_{P2}. The magnitude of S in low-Ohmic samples at $T < T_{P2}$ is well below $k_B/e \approx 86\ \mu$V/K, k_B being the Boltzmann constant and e the elementary charge, which is surprisingly low for a usual CDW semiconducting state. Our results suggest that at T_{P1} the main electronic band with p-type carriers becomes gapped, while some n-type carriers can remain in a separate band with low density of states. These carriers, whose concentration is defined by the compositional doping, are gapped at T_{P2}. We also report S for the triclinic dielectric phase of NbS_3 (NbS_3-I). Its low absolute value, $\sim k_B/e$, and the anomalous temperature dependence demonstrate that NbS_3-I is neither a semiconductor nor a CDW conductor in the usual sense.

DOI: 10.1103/PhysRevB.99.235155

I. INTRODUCTION

The quasi-one-dimensional compound NbS_3 is known to condense in two forms: the triclinic (phase I) and monoclinic (phase II) [1,2], though other forms have been recently reported [3]. Phase II (or NbS_3-II) reveals extremely rich physics [1,2,4,5], showing three charge density wave (CDW) transitions: at $T_{P0} \approx 460$ K [4,6,7], at $T_{P1} = 360$ K, and at $T_{P2} = 150$ K . Below, the corresponding CDW phases are referred to as CDW-0, CDW-1, and CDW-2.

The remarkable feature of NbS_3-II is that the crystals with the same structure show diverse properties, which can be tuned by the growth conditions [4,8–11]. The room-temperature specific conductivity of the samples, σ_s, varies from 3×10^2 (low-Ohmic samples) down to $2(\Omega\ \mathrm{cm})^{-1}$ (high-Ohmic samples [4]), or even to $\sim 0.1\ (\Omega\ \mathrm{cm})^{-1}$ [10]. The low-Ohmic samples are found to be sulfur deficient [4]. It has been suggested that in such samples sulfur vacancies behave as donors and give rise to extra "doping-induced" electrons [4]. The details of NbS_3-II structure and of its charge density modulations have been recently reported [12,13] and show that different CDW modulations appear in different chains in the unit cell.

The T_{P0} transition is characterized with a lattice distortion with $q_0 = (0.5a^*, 0.352b^*, 0)$ [4,14] and gaps the electrons in the band belonging to one pair of chains in the unit cell [12]. Like the T_{P0} transition, the transition at T_{P1}, which gaps the band in another pair of chains, is believed to be a Peierls transition in the usual sense, showing a lattice distortion with the wave vector $q_1 = (0.5a^*, 0.298b^*, 0)$ and a steplike feature in the $\sigma_s(T)$ curve [1,2,4]. However, the dielectrization at T_{P1} can be incomplete. The scattering in σ_s between different samples grows drastically below T_{P1} [4] [see also Fig. 1(a)]. While the high-Ohmic samples become completely dielectrized at T_{P1}, the doping-induced electrons are likely to dominate the conductivity in the low-Ohmic samples down to T_{P2}.

The nature of CDW-2 is still under discussion [4]. No extra lattice distortion has been revealed below T_{P2} by structural studies. Like CDW-1 and CDW-0 [4,7], CDW-2 shows threshold nonlinear conduction and Shapiro steps under RF field. Thus, there is no doubt that the electronic condensate forming at T_{P2} is a kind of CDW. However, the charge density transferred by CDW-2, found from the Shapiro steps analyses [4], appears extremely low and sample dependent. Thus CDW-2 has been suggested to be a condensate of the doping-induced electrons, probably an excitonic insulator [4].

*pok@cplire.ru
†wpai@ntu.edu.tw

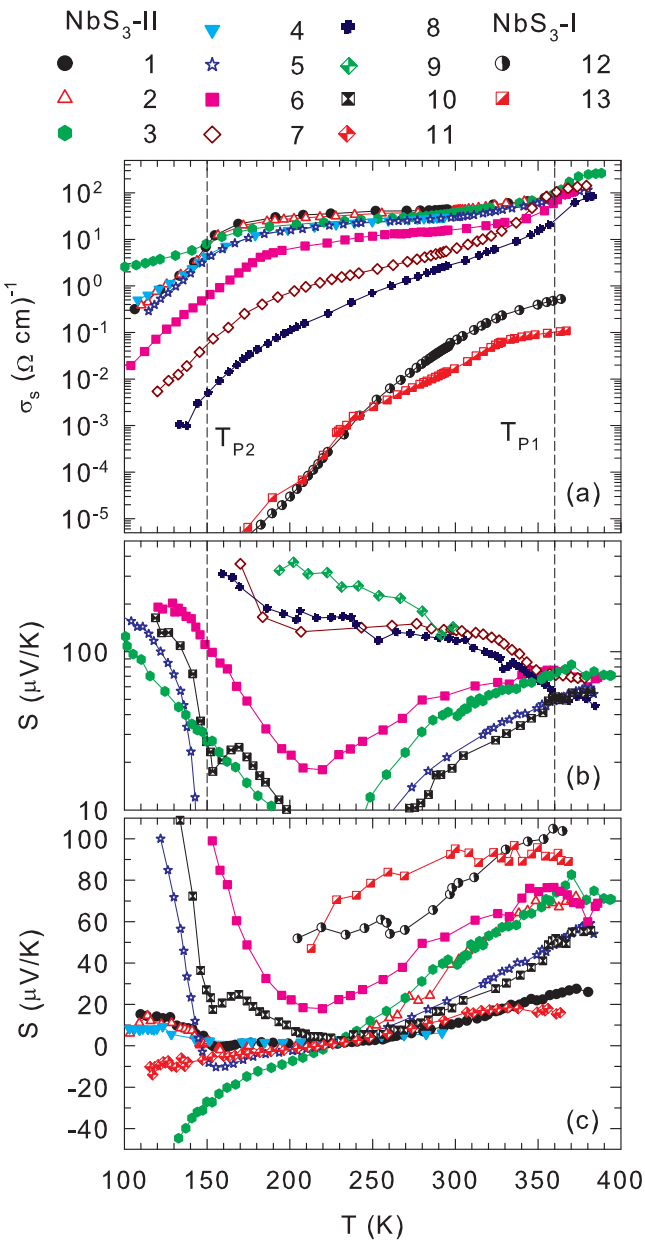

FIG. 1. (a) The $\sigma_s(T)$ dependencies for NbS_3-II (samples 1–8) and NbS_3-I (samples 12, 13). The symbols show a small part of the experimental points. Two lowest curves with half-filled symbols show σ_s for NbS_3-I samples. Full symbols show samples for which the dimensions have been measured: for NbS_3-II samples 1, 3, 4, 6, and 8 using RF interference and for NbS_3-I samples 12 and 13 optically. Empty symbols show samples 2, 5, and 7 for which the specific conductivity has been estimated based on $\sigma_s(T)$ dependence (see Sec. III B). (b) $S(T)$ dependence for NbS_3-II samples whose $S(T)$ grows below T_{P2}. For sample 3 the absolute value of negative $S(T)$ at low temperature is given. For samples 9 and 10, whose $\sigma_s(T)$ has not been measured, data are shown with checkered symbols. (c) $S(T)$ dependence for NbS_3-II samples whose $S(T)$ decreases with temperature below T_{P1} and for two NbS_3-I samples. For samples 10 and 11, whose $\sigma_s(T)$ has not been measured, data are shown with partially filled symbols. The range is reduced, so that details close to $S = 0$ can be observed. Data outside this range, for samples whose $S(T)$ grows below T_{P2}, are shown in (b). Note that neither panel (b) nor panel (c) shows all the $S(T)$ curves. The vertical dashed lines in all panels indicate nominal positions of the CDW transition temperatures T_{P1} and T_{P2}.

A somewhat similar behavior has been also reported for the samples with an excess of sulfur [9,10]. In all the cases, the control of the composition was estimative, and a more detailed study of NbS_3-II properties versus composition is desirable [15].

In view of the cascade of CDW transitions, one can expect a complex structure of electronic energy gaps in NbS_3-II. The most high-Ohmic samples show the activation energy of about 2000 K below T_{P1} [4]. This value is close to 2500 K, the half value of optical gap reported for NbS_3-II [16].

One can clearly distinguish phase I (or NbS_3-I) from phase II based on its conducting and structural properties. Though the elementary cell of NbS_3-I comprises only two Nb chains, in contrast to eight chains in the cell of phase II [1,2,12,17,18], the doubling along the chains' direction (b axis) reduces the symmetry of the crystalline structure down to the triclinic group. This compound is in a dielectric state already at room temperature, with $\sigma_s \sim 10^{-2}$ $(\Omega\ \mathrm{cm})^{-1}$ [1,2]. The reported low-temperature activation energy for conductivity varies from 3800 K (0.33 eV) [19] to 4400 K (0.38 eV) [14]. Transmittance measurements give the optical energy gap $2\Delta_o = 0.68$ eV at 298 K [19] and 0.83 eV at 8.5 K [20]. Photoconduction measurements reveal the temperature-dependent optical gap varying from $2\Delta_o = 0.85$ eV ($T = 220$ K) to 1.08 eV ($T = 5$ K) [21]. In addition, the optical measurements indicate the presence of in-gap states [20] that are sensitive to temperature, electric field, and illumination intensity [21]. The origin of the dielectric state in NbS_3-I is still not well understood.

The Seebeck coefficient S is one of the most sensitive probes of the electronic band structure in the system [22]. It provides the sign of the majority carriers and can clearly distinguish between characteristic behaviors for metals, semiconductors, superconductors, etc. However, when multiple conducting bands and/or carrier scattering mechanisms are involved, the interpretation of data becomes more complex and allows typically only qualitative understanding. In CDW systems the Seebeck coefficient below T_P can be roughly described by analogy with that in semiconductors [23–27]. In the completely dielectrized state the values of S are typically on the order of $(k_B/e)(\Delta/T)$, where Δ is the half-width of the Peierls gap, k_B the Boltzmann constant, and e the elementary charge. A more detailed semiconductor model can also describe the main features of thermopower and conductivity and their correlations for compounds with different electron-hole balance, where these properties are sensitive to the position of the chemical potential within the gap (see Ref. [28] and references therein). At the same time, significant deviations of S from the values predicted by the semiconductor model occur both at moderate [23,27,29] and low [24–26,30] temperatures.

In this paper we report studies of thermopower on both phases of NbS_3. For phase II the $S(T)$ curves clearly reveal the gaps opening at T_{P1} and T_{P2} and appear rather sensitive to the concentration of doping-induced electrons. The behavior of $S(T)$ and $\sigma_s(T)$ for different concentrations of the extra electrons is described within a model with multiple bands. For

phase I the $S(T)$ studies show that the electronic states in this dielectric compound cannot be treated within the models of a conventional semiconductor.

II. EXPERIMENTAL TECHNIQUES

Synthesis of NbS_3-I was worked out in the 1970s [31]. The conditions of reproducible synthesis of NbS_3-II samples were established not long ago [8], and their properties were recently systematized in [4]. For the present studies samples with different σ_s have been selected. On average, the higher-Ohmic samples were found in the higher-temperature part of the "cocoon" removed from the growth ampoule [4].

Because NbS_3 samples grow as thin whiskers with cross-sectional area $s \sim 10^{-1}$ to 10^{-2} μm^2 and length L between several tens and hundreds of microns, special techniques were developed for the challenging S measurements. Short samples were placed on sapphire substrates. One end of the substrate was thermally grounded. A tiny heater placed near the other end was used to create an approximately linear temperature distribution along the substrate, and the temperature change along the sample was calculated based on its length. The temperature variation of the grounded end of the substrate was negligible.

A better accuracy of thermoelectric voltage measurements was achieved for samples with $L > 100$ μm. In this case the sample was placed on a mica substrate between massive indium contacts. One of the contacts was thermally grounded, while the other one was heated. The heater and a platinum thermometer were stuck to this contact. Thus, the temperature was controlled directly at the contact.

In the course of measurements the heater was periodically switched on and off for a time interval sufficient for the formation of stationary temperature distribution. The typical temperature difference between the sample ends was about 0.5 K. At low temperatures it was increased sometimes to improve signal-to-noise ratio, but did not exceed 5 K. In all the cases, the temperature drop along the sample was small enough to avoid distortions of the $S(T)$ curves around sharp features. The thermoelectric voltage was measured with a Keithley 2000 multimeter across samples with resistance below $\sim$1 GΩ. For testing the technique we have studied $S(T)$ of the TaS_3 samples [29]. In the temperature range 70–300 K the S values appeared in good agreement with [23] and a little bit below those reported in Ref. [27], where the measurements were performed on samples synthesized in the same group (the Thorne group). Similarly, S values of the TiS_3 whiskers [29] appeared close to the results of Ref. [32] at $T = 200$–300 K, where $S = -(600$–$800)$ μV/K is roughly sample independent [29].

The conductivity σ was measured for the same samples, by the two-probe technique between the same contacts. Because the properties of the NbS_3-II samples strongly correlate with their *specific* conductivity σ_s [4], it was important to know not only the conductivity value but also the samples' dimensions. The effect of RF synchronization of CDW-1 sliding allowed determination of the cross-section areas and, thus, σ_s for most of the samples [4,33]. The transverse dimensions of the NbS_3-I samples were relatively large and were estimated from the studies under an optical microscope.

Some of the samples were damaged during σ measurements, so we were not able to determine their cross-section areas directly by RF synchronization. However, in Sec. III B, Fig. 3(c), we show that for samples with known cross section, the effective activation energy E_{act} depends monotonically on the room-temperature specific conductivity σ_{RT}. Therefore we have estimated the cross-section areas of damaged samples so that their E_{act} vs σ_{RT} values conform to the same dependence.

The heat capacity was measured by a PPMS instrument (Quantum Design, Inc.) in the temperature range 2 K to 375 K. A pellet of 6.2 mg mass was obtained by pressing a large number of NbS_3-II whiskers from a batch of samples similar with those used for thermopower studies.

III. RESULTS

A. Overview of electric conductivity and thermopower

Temperature dependence of the Seebeck coefficient $S(T)$ was measured on altogether 11 samples of NbS_3-II and two samples of NbS_3-I. Temperature dependence of the electric conductivity $\sigma_s(T)$ was successfully measured for eight of these NbS_3-II samples and both NbS_3-I samples. The cross section was determined by RF synchronization on five of these eight NbS_3-II samples. For the other three samples the cross section has been estimated as described in Sec. III B. The parameters determined for the samples are presented in Table I.

Figure 1 presents the $\sigma_s(T)$ and $S(T)$ data for all measured samples. For the same sample, identical symbols are used for $\sigma_s(T)$ in Fig. 1(a) and $S(T)$ in Figs. 1(b) and 1(c). $\sigma_s(T)$ for the samples with estimated cross-section areas (see Table I and Sec. III B) are represented by empty symbols. In Figs. 1(b) and 1(c) the $S(T)$ curves for NbS_3-II samples 9–11, whose $\sigma(T)$ dependencies have not been measured, are denoted with checkered symbols. $\sigma_s(T)$ and $S(T)$ data for NbS_3-I samples 12 and 13 are denoted with half-filled symbols.

1. Electric conductivity and thermopower of NbS_3-II

In general, the set of $\sigma_s(T)$ curves of NbS_3-II samples in Fig. 1(a) is consistent with that reported in [4], though the number of samples studied here is smaller and the range of their σ_s values is narrower. However, here $\sigma_s(T)$ has been systematically measured for multiple samples across the CDW transition at T_{P1}. It seems that T_{P1} does not vary much between the samples and that σ_s for different samples shows far less divergence above than below T_{P1}.

The phase-II samples show features in $\sigma_s(T)$ around both $T_{P1} \approx 360$ K and $T_{P2} \approx 150$ K. Going from low-Ohmic to high-Ohmic samples one can see obvious tendencies: the lower σ_s is, the steeper it decreases with temperature decrease and the less pronounced is the feature at 150 K. That is, the CDW-2 tends to appear in low-Ohmic samples.

The $S(T)$ curves [Figs. 1(b) and 1(c)] show much more diverse behavior than the $\sigma_s(T)$ curves, as has been remarked in Ref. [10]. At high temperatures $S(T)$ is positive, indicating p-type conductivity, of the order of k_B/e, which is too large for ordinary metallic conduction mechanisms [22]. However, as temperature decreases, $S(T)$ is observed to either increase or decrease, and even change sign in different samples.

In the high-Ohmic samples 7 and 8 [Fig. 1(b)], $S(T)$ increases stepwise at T_{P1} and then even more strongly near T_{P2}. In sample 9 $S(T)$ continuously increases already below

TABLE I. Numbered list of all investigated NbS_3 samples, together with different parameters that characterize them: length L, cross section s, room-temperature specific conductivity σ_{RT} and Seebeck coefficient S_{RT}, high-temperature specific conductivity σ_{HT}, CDW transition temperatures T_{P1} and T_{P2}, E_{act} and σ_0 obtained from the fit of $\sigma_s(T)$, and δS and S_0 obtained from the fit of $S(T)$. The s and σ_{RT} values marked with * are estimated to conform to the smooth dependence of E_{act} on σ_{RT}, as presented in Fig. 3(c). The activation energy E_{act} and preexponential constant σ_0 are obtained from the fit of $\sigma_s(T)$ to Eq. (1), $\sigma(T) = \sigma_0 \exp(-E_{act}/k_B T)$. The linear coefficient δS and constant S_0 are obtained from the fit of $S(T)$ to Eq. (4), $S(T) = S_0 + \delta S \times T$.

	Sample	L (μm)	s (μm^2)	T_{P1} (K)	T_{P2} (K)	σ_{RT} $(\Omega\ \mathrm{cm})^{-1}$	σ_{HT} $(\Omega\ \mathrm{cm})^{-1}$	S_{RT} (μV/K)	E_{act} (K)	σ_0 $(\Omega\ \mathrm{cm})^{-1}$	δS (μV/K^2)	S_0 (μV/K)
	1	126	0.063	364	149	43	147	9.7	255	113	0.2	−48.5
	2	300	0.17*	367	146	40*	221	36.8	259	100	0.63	−151.5
	3	210	0.11	367	151	34	267	41.2	284	85	0.53	−118.3
	4	50	0.12		147	30		30.2	417	129		
	5	72	0.063*	360	143	29*	122	21.6	413	125	0.38	−89.6
NbS_3-II	6	210	0.19	360	171	16	111	53.1	683	184	0.44	−79.7
	7	400	0.11*	346	150	5.5*	146	138	1160	232		
	8	100	0.012	367	170	2.6	84	121	1760	724		
	9	140						135				
	10	250						17.6			0.36	−86.5
	11	80						12.9			0.15	−32.1
	12	1260	245			0.046	0.53	72	4580	2.5×10^5	0.38	−34.9
NbS_3-I	13	1000	100			0.014	0.11	91.8				

T_{P1}. The thermopower measurements on these high-Ohmic samples could not be performed properly below T_{P2} since the resistance exceeded 1 GΩ.

In low-Ohmic samples [Fig. 1(c)], on the other hand, $S(T)$ curves start to go down below T_{P1}, converge to a value $S \sim 0$ at $T_i \sim 225$ K, and even cross to negative values below T_i. Such intersections of curves with varying parameter have been observed for different physical quantities and are sometimes referred to as "isosbestic" points [34].

Though $\sigma_s(T)$ has not been measured for samples 10 and 11, we have included them in the low-Ohmic group, as they show decreasing $S(T)$ curves below T_{P1}.

Apparently, the temperature dependence of both S and σ_s can be, at least roughly, classified according to the absolute value of σ below T_{P1}, i.e., around room temperature. We will thus use the room-temperature conductivity σ_{RT} to parametrize different samples in subsequent analysis of $S(T)$ and $\sigma_s(T)$ of NbS_3-II.

From the comparison of our results with Ref. [10] we notice that the $\sigma(T)$ curves for the samples with "closely stoichiometric" composition (batch B in [10]) resemble the curves for the high-Ohmic samples [Fig. 1(a)]. Correspondingly, the curves for "sulfur-rich" samples (batch A in [10]) look like the curves for the low-Ohmic samples [Fig. 1(a)]. However, the samples labeled B [10] show a change of sign in the $S(T)$ curves, in contrast to our high-Ohmic samples. At the same time, the $S(T)$ curves for A samples look like those for the low-Ohmic ones in Fig. 1(b). Thus, in spite of the similarity of the absolute values and temperature dependencies of S in Ref. [10] and in the present paper, one should be very careful in comparison of the results. Presumably, higher accuracy in the composition determination is required.

$S(T)$ dependences for low-Ohmic samples around and below T_{P2} appear rather sample specific. Most of the low-Ohmic samples show steplike increase at T_{P2}; in three samples with lower σ_{RT} (samples 5, 6, and 10), $S(T)$ grows without saturation, similarly to high-Ohmic samples. For samples with higher σ_{RT} (samples 1, 2, and 4), $S(T)$ only slowly increases at lower temperatures. Two samples (3 and 11) do not show any feature near T_{P2} and their $S(T)$ remains negative at low temperatures. Sample 3, which has somewhat nonsystematic $\sigma_s(T)$ below T_{P2} [35], shows decreasing and negative S below T_{P2}.

Regardless of all the variations in $S(T)$ between the samples, the values of S correlate with the values of σ_s. This is shown in Fig. 2, in which S is plotted versus σ_s for different samples at several temperatures; the samples with higher σ_s show lower S. The correlation can be seen already at 335 K, slightly below T_{P1}, and it persists down to 135 K, i.e., below T_{P2}.

2. *Electric conductivity and thermopower of* NbS_3-I

The $\sigma_s(T)$ curves of the NbS_3-I samples can be clearly distinguished in Fig. 1(a). At high temperatures phase I shows

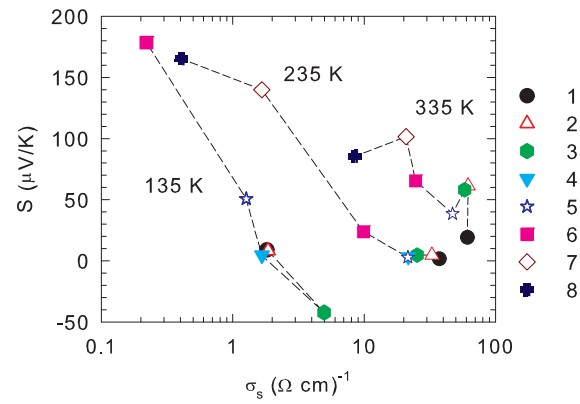

FIG. 2. S as a function of σ_s for different samples at selected temperatures: near T_{P1}, between T_{P1} and T_{P2}, and below T_{P2}. Empty symbols are used for samples for which σ_s has been estimated based on $\sigma_s(T)$ dependence (see Sec. III B).

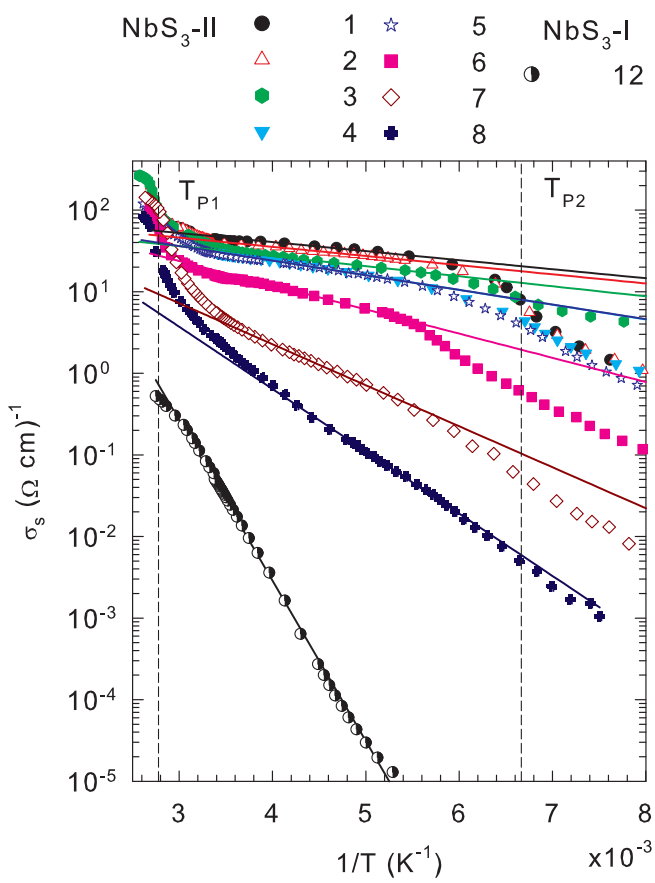

FIG. 3. Arrhenius plot of $\sigma_s(T)$ for NbS_3-II samples and for NbS_3-I sample 12 (lower black line). The symbols show a small part of the experimental points. Straight lines represent the results of the fits to the activated behavior, Eq. (1), in the temperature range 200–300 K (see text). The vertical dashed lines indicate nominal positions of the CDW transition temperatures T_{P1} and T_{P2}.

more than 2 orders of magnitude lower conductivity, and it decreases much faster with the temperature than $\sigma_s(T)$ of the NbS_3-II samples, in agreement with the semiconducting nature of this phase [14,19]. However, above room temperature $\sigma_s(T)$ grows much slower, suggesting saturation at high temperatures. We will further analyze sample 12, as sample 13 shows some unusual and unexpected undulations in temperature dependence of conductivity around 300 K and approaches $\sigma_s(T)$ of sample 12 only at low temperatures.

Thermopower for these samples could be measured only down to 200 K, until R exceeded ~1 GΩ. At room temperature the S values are close to those of NbS_3-II [Fig. 1(c)]. While σ_s decreases at low T, the S values do not grow, but even decrease in the range 360–200 K. Thus, the behavior of $S(T)$ in NbS_3-I is not typical for normal semiconductors.

B. Analysis of the conductivity of NbS_3

Figure 3 shows the Arrhenius plot [$\log(\sigma_s)$ vs $1/T$] of NbS_3-II $\sigma_s(T)$ data; low- and high-Ohmic samples can be clearly distinguished [4]. Apparently, in the temperature range between T_{P1} and T_{P2}, $\sigma_s(T)$ shows an activated behavior,

$$\sigma(T) = \sigma_0 \exp\left(-\frac{E_{act}}{K_B T}\right), \quad (1)$$

where E_{act} is the activation energy and σ_0 is preexponential factor. Straight lines in Fig. 3 represent the results of the fits to Eq. (1) in the temperature range 200–300 K. The $\sigma_s(T)$ curves of low-Ohmic samples show steplike decrease with cooling at both transition temperatures. For high-Ohmic samples, the steplike feature is absent and only a slight deflection from the activated behavior might be observed near T_{P2} [4].

We have extracted the values of T_{P1} and T_{P2} from the positions of inflection points in $\log \sigma_s(T)$ vs $1/T$. We have also extracted the high-temperature values of σ_s for different samples, σ_{HT}, obtained at temperatures slightly above the steplike increase at T_{P1}. Although these temperatures are not the same for different samples, the temperature dependence of σ_s is rather flat above T_{P1}, so rough comparison can be made.

The parameters obtained from $\sigma_s(T)$—E_{act}, σ_0, σ_{HT}, T_{P1}, and T_{P2}—are given in Table I and presented as a function of σ_{RT} in Fig. 4. Data for five samples for which exact values of σ_s have been obtained from RF synchronization are shown with full symbols.

Here T_{P1} and σ_{HT} have been determined for a number of samples. With a few exceptions, T_{P1}, presented in Fig. 4(a), is in the range of 360–370 K and T_{P2}, presented in Fig. 4(b), is in the range of 140–150 K, regardless of the σ_{RT} value.

Both E_{act} and σ_0 increase by almost an order of magnitude as σ_{RT} decreases. This variation is more pronounced for smaller σ_{RT} values. E_{act} eventually reaches the value close to that reported for the most high-Ohmic samples, about 2000 K [4]. The dependence of E_{act} on σ_{RT} is almost linear in log-log scale, as shown in Fig. 4(c). We have used this feature to estimate σ_{RT}, and therefore $\sigma_s(T)$, for samples for which proper cross section was not measured. On the other hand, σ_0 values vary within a somewhat narrower range of values, 100–200 $(\Omega\ \mathrm{cm})^{-1}$, except for the sample with lowest σ_{RT}. Finally, while σ_{RT} varies by almost 2 orders of magnitude, σ_{HT} shows a nonsystematic variation by only a factor of 3 between the samples.

In the simplified model of semiconductors, E_{act} represents the chemical potential, i.e., the difference between the position of the Fermi level, E_F, and the closest band edge, either conduction E_C or valence E_V: $E_{act} \approx |E_F - E_{C(V)}|$. Only for an intrinsic semiconductor is E_{act} equal to the half-width of the band gap Δ. On the other hand, for an extrinsic semiconductor in the low temperature ionization regime E_{act} is constant and equal to the half of the dopant ionization energy. Thus, the variation of E_{act} between different samples can be interpreted as the change of the position of E_F within CDW gap due, for example, to the doping by sulfur deficiency [4]. However, specifically for collective electron-phonon states like CDW, the value of the gap can also change with doping [36] while the temperature variation of the CDW wave vector $q(T)$ can create intrinsic electron-hole imbalance [28] and affect E_{act} [37,38].

NbS_3-I sample 12 shows activated behavior in the entire range below ~300 K, as presented in Fig. 3, with some flattening at higher temperatures. The obtained $E_{act} \approx 4600$ K is within the range of previously reported values [14,19].

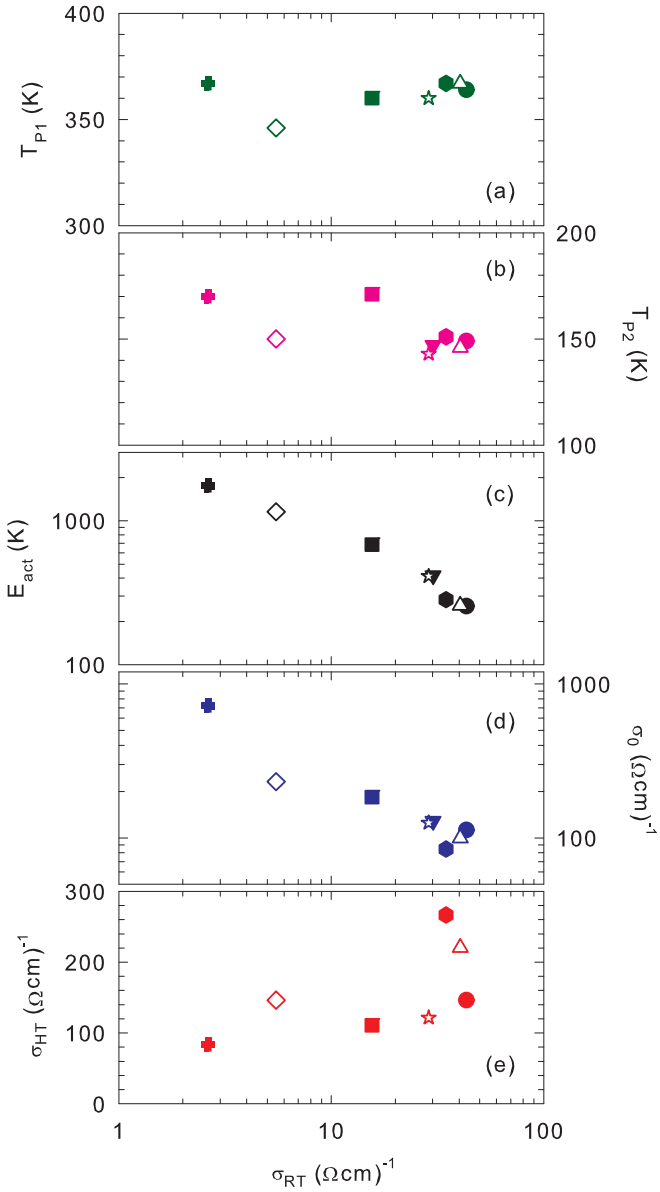

FIG. 4. Different parameters extracted from $\sigma_s(T)$ using Eq. (1) as a function of σ_{RT}: (a) T_{P1}, (b) T_{P2}, (c) E_{act}, (d) σ_0, (e) σ_{HT}. Full symbols are for samples for which the cross section has been measured and therefore the exact value of σ_s is known. Empty symbols are for samples for which σ_{RT}, and consequently $\sigma_s(T)$, has been set to conform with the value of E_{act} (see text).

C. Analysis of the thermopower of NbS_3

The analytical equations for the Seebeck coefficient can be derived in the degenerate limit, Eq. (2), appropriate for metals and highly doped semiconductors, and in the nondegenerate limit, Eq. (3), appropriate for intrinsic and lightly doped or compensated semiconductors [39]:

$$S(T) = \frac{k_B}{Q}\left(r + \frac{3}{2}\right)\frac{\pi^2}{3}\frac{1}{\eta}, \tag{2}$$

$$S(T) = \frac{k_B}{Q}\left(r + \frac{5}{2} - \eta\right). \tag{3}$$

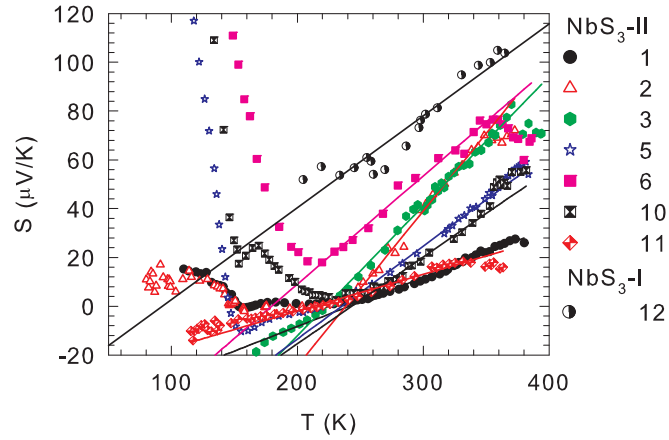

FIG. 5. Linear fit, Eq. (4), of the temperature dependence of $S(T)$ in the temperature range 250–350 K for low-Ohmic samples of NbS_3-II and one NbS_3-I sample. The symbols for different samples are the same as in Fig. 1.

In both equations, r is the parameter determined by the energy dependence of electron scattering, typically between -0.5 and 1.5, Q is the charge of the carriers, which gives negative S for electrons ($Q = -e$) and positive S for holes ($Q = e$), while η is the reduced electron (or hole) chemical potential, $\eta = (E_F - E_C)/k_BT$ [$\eta = (E_V - E_F)/k_BT$].

For low-Ohmic samples, S decreases with temperature decrease from T_{P1} down to T_i(225 K), and $S(T)$ can be fitted with the linear function,

$$S(T) = S_0 + \delta S \times T, \tag{4}$$

as shown in Fig. 5. The parameters S_0 and δS obtained from the fit are given in Table I and presented Fig. 6. The parameters do not show any clear systematic variation with σ_{RT}, but they do not differ substantially between the samples either.

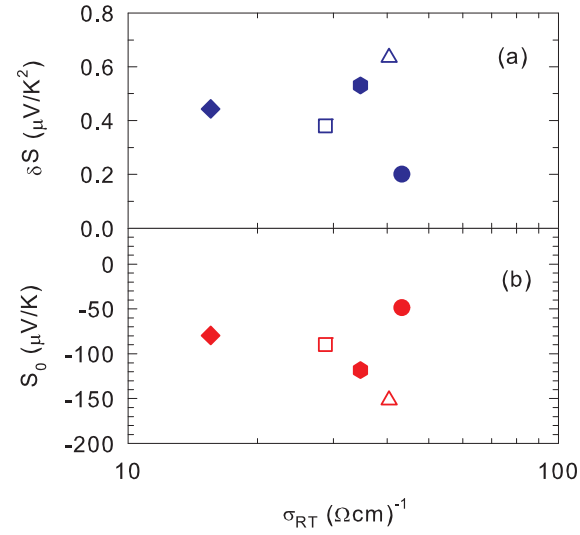

FIG. 6. Different parameters extracted from linear fit of $S(T)$, Eq. (2), as a function of σ_{RT}: (a) δS, (b) S_0. Different symbols correspond to different samples and are the same as in Fig. 1 and Fig. 5. Empty symbols are used for samples for which σ_{RT} has been estimated based on $\sigma_s(T)$ dependence (see Sec. III B).

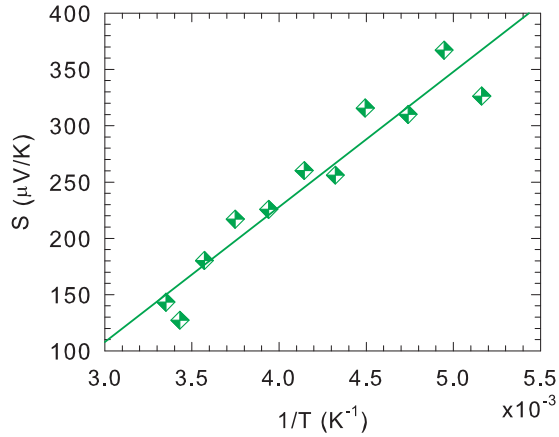

FIG. 7. S of sample 9 as the function of the inverse temperature $1/T$. The line is the fit to Eq. (3).

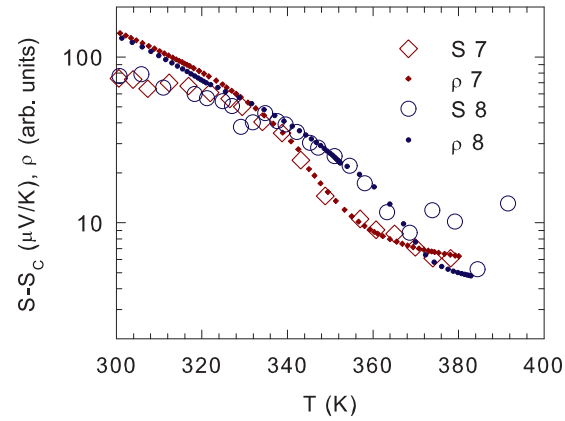

FIG. 8. Comparison of the temperature dependence of rescaled thermopower S and resistivity ρ for two high-Ohmic samples, 7 and 8. For sample 7, $\rho(\text{arb.}) = 800/\sigma_s(T)$ ($\rho \times 800$, Ω cm) and $S_c = 62$ μV/K, while for sample 8, $\rho(\text{arb.}) = 400/\sigma_s(T)$ ($\rho \times 400$, Ω cm) and $S_c = 40$ μV/K.

If we consider that the linear T dependence of S is defined by η as in Eq. (2), ηT would be on the order of 10^3 K, much lower than in metals (10^4–10^5 K). Therefore E_F would be close to E_V, as in degenerate semiconductors and semimetals [40]. On the other hand, the negative and large (on the order of k_B/e) value of S_0 is not obtained in the simple theory for metals and highly doped semiconductors.

As presented in Fig. 5, $S(T)$ of NbS_3-I sample 12 can also be roughly fitted by Eq. (4) with S_0 and δS values, similarly to the low-Ohmic NbS_3-II samples.

S strictly increases at low T in sample 9, for which $\sigma_s(T)$ has not been measured. Presented as a function of inverse temperature in Fig. 7, its $S(T)$ seems to follow the temperature dependence given by Eq. (3). The fit, represented by the line in Fig. 7, gives $E_F - E_V \approx 1400$ K, which is close to E_{act} obtained for the high-Ohmic samples. Also the value of $r + 5/2 \approx -3$ obtained from the fit has a reasonable magnitude, but its negative sign would not be expected for a simple hole contribution to S.

For the two high-Ohmic samples 7 and 8, S shows a strong increase only around T_{P1} [whose correlation with $\sigma_s(T)$ we analyze in the following section], but then remains nearly constant almost down to T_{P2}. If we try to analyze it with simple expressions given in Eq. (2) and Eq. (3), the only possibility would be to use $\eta \approx 0$ in Eq. (3), corresponding to the Fermi level situated near the top of the valence band ($E_F \approx E_V$).

It is evident that the $S(T)$ curves of the low-Ohmic and high-Ohmic samples of NbS_3-II below T_{P1} are qualitatively similar to those expected for degenerate and nondegenerate semiconductors, respectively. The crossover from degenerate to nondegenerate $S(T)$ with decreasing σ_{RT} is also consistent with the concurrent increase of E_{act} obtained from $\sigma_s(T)$ analysis. However, fits to the simplified equations give large negative constant contributions that cannot be understood within the simple unipolar holelike conductivity model.

D. Correlation of thermopower and conductivity in NbS_3-II around T_{P1}

As we noted before, in the high-Ohmic samples $S(T)$ shows a steplike increase at T_{P1}, similarly to the steplike decrease in $\sigma_s(T)$. The correlation between the conductivity and thermopower at the CDW transition has already been noticed in another CDW system, o-TaS_3 [27], where a scaling between $S(T)$ and $\rho(T) \equiv 1/\sigma_s(T)$ can be observed. In Fig. 8, we present $\rho(T)$ scaled by a suitable factor together with $S(T)$ for the two high-Ohmic samples 7 and 8. Constant values S_C have been subtracted from $S(T)$ to highlight the steplike increase at T_{P1}. The scaling works well for both samples; e.g., the small difference in T_{P1} of the two samples is seen both in $S(T)$ and $\rho(T)$.

It has been shown that in o-TaS_3 the behavior of the basic characteristics near T_P, namely, of conductivity, thermal expansion, elastic moduli, specific heat [41], and threshold field [42], can be well described with a semiempirical model of spontaneous phase slippage (PS). This model describes the transition as the growth of the fraction $\mathbf{f}$ of the normal phase through the local CDW gap suppression ("phase slip") with increasing T. Thus the total resistivity ρ is composed of contributions from the $\mathbf{f}$ fraction with normal-state resistivity ρ_n and $1 - \mathbf{f}$ fraction of CDW state with the resistivity ρ_c:

$$\rho = \mathbf{f} \cdot \rho_n + (1 - \mathbf{f}) \cdot \rho_c. \quad (5)$$

A similar relation can be written for the thermopower of a system consisting of two fractions with different properties [43]:

$$S = \frac{S_n \cdot \mathbf{f} \cdot \kappa_n + S_c \cdot (1 - \mathbf{f}) \cdot \kappa_c}{\mathbf{f} \cdot \kappa_n + (1 - \mathbf{f}) \cdot \kappa_c} \approx S_n \cdot \mathbf{f} + S_c \cdot (1 - \mathbf{f}). \quad (6)$$

Here κ denotes the thermal conductivity and the indices "n" and "c" indicate the normal and the CDW states, correspondingly. As the electronic contribution to κ is negligible in systems with low electronic conductivity, the values of κ_n and κ_c are the same, and S depends only on the fractional contributions of the normal and the CDW states. The dominant contribution to the temperature variation in Eqs. (5) and (6) in the region of the Peierls transition thus comes from the temperature dependence of $\mathbf{f}$, which can explain the scaling between $R(T)$ and $S(T)$.

The temperature dependence of $\mathbf{f}$ can be numerically determined from $\rho(T)$ according to Eq. (5) using analytical expressions for $\rho_c(T)$ and $\rho_n(T)$. For $\rho_c(T)$ we have used the

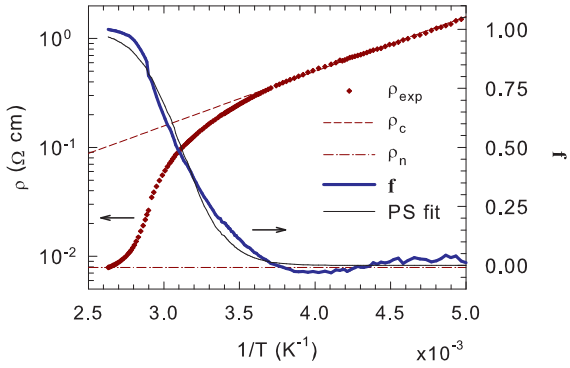

FIG. 9. The solid thick line shows numerical evaluation of the fraction **f** of the normal phase for sample 7, based on the phase slippage model, Eq. (5), using experimental $\rho(T)$ values, activated dependence of $\rho_c(T)$, and constant $\rho_n(T)$. The thin full line represents the fit of $\mathbf{f}(T)$ to the theoretical expression derived for PS process in Eq. (7).

previously determined activated dependence [Eq. (1), Figs. 3 and 4], while $\rho_n(T)$ has been simply taken to be constant and equal to the high temperature $\rho(T)$. We have evaluated **f** for all samples and an example for high-Ohmic sample 7 is shown in Fig. 9. Moreover, the $\mathbf{f}(T)$ curve around T_{P1} can be well approximated with the theoretical expression derived for the PS process [41]:

$$\mathbf{f} = \frac{1}{1 + a\exp(W/T)}, \tag{7}$$

with the barrier for thermally activated PS $W \approx 7000$ K, as represented with the full line in Fig. 9.

We were able to reconstruct quite well the temperature dependence of $S(T)$ around T_{P1} for all NbS_3-II samples using numerically estimated values of $\mathbf{f}(T)$ in Eq. (6), as shown in Fig. 10 for several selected high-Ohmic and low-Ohmic samples. We have simply used the constant high temperature value of S for S_n. For S_c we have used the previously determined linear dependence [Eq. (4), Figs. 5 and 6] for the low-Ohmic samples and constant values for the high-Ohmic

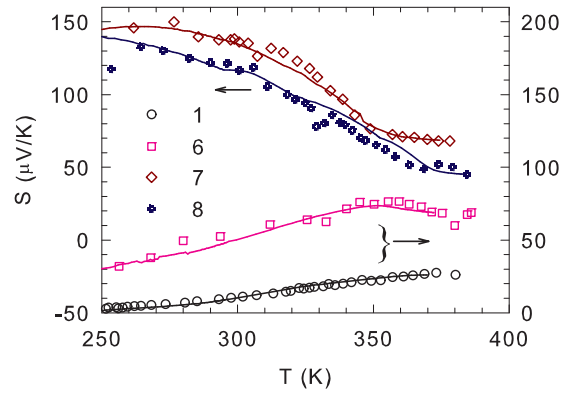

FIG. 10. Comparison of the temperature dependence of S around T_{P1} with the estimates based on the phase slippage model [Eq. (6)] using the numerically evaluated fraction **f** of the normal phase and experimentally determined $S(T)$ sufficiently above and below T_{P1} (see text).

samples equal to the values of S at 200 K, i.e., sufficiently below T_{P1}, but still higher than T_{P2}.

Our analysis shows that the phase slippage model [41] of the CDW transition, or, more generally, a model suggesting growing of the normal phase within the CDW phase, can be applied to describe $S(T)$ around the CDW transition at T_{P1} in both the high- and low-Ohmic NbS_3-II samples.

E. Semiconductor model of thermopower and conductivity in NbS_3-II between T_{P1} and T_{P2}

As we have already noted, $S(T)$, and particularly its change of sign at low temperatures, suggests contributions from both electrons and holes below T_{P1}. In this section we take this into account and try to model both $S(T)$ and $\sigma_s(T)$ consistently within a semiconductor model that takes into account the contributions from both electrons in the conducting band and holes in the valence band as well as possible doping.

We will use the integral solutions of the Boltzmann equation in the relaxation time approximation [39,44] for $S(T)$ and $\sigma_s(T)$. For both conduction and valence band we adopt simple quadratic dispersion relations parametrized by generally different effective band mass for electrons in the conduction band, m_C, and holes in the valence band, m_V. We also adopt a simple expression for the energy and temperature dependence of the relaxation time τ, $\tau(T,E) = \tau_0 T^{-1} E^{-1/2}$, appropriate for the scattering of the electrons by acoustic phonons in the high-temperature limit [45].

The CDW gap in NbS_3-II is comparable to the thermal energy, $k_B T$. For such narrow-gap semiconductors, even if the gap value $\Delta \equiv E_C - E_V$ is constant, the (reduced) chemical potential η can vary strongly with temperature, both due to the different effective density of states $N_{C(V)}$ in the conduction (valence) band and due to the doping. Generally, at each temperature η should be determined by the charge neutrality requirement [46]:

$$N_c \mathcal{F}_{1/2}(\eta) - N_v \mathcal{F}_{1/2}(-\Delta - \eta) = N_r, \tag{8}$$

where N_r is the density of extra carriers provided by doping. The positive values of N_r represent electron doping, while negative values hole doping. $N_{C(V)}$ is the effective density of states at the bottom (top) of the conduction (valence) band:

$$N_{C(V)} = 2\left(\frac{2\pi m_{C(V)} k_B T}{h^2}\right)^{3/2}, \tag{9}$$

where $m_{C(V)}$ are the effective electron and hole masses at the bottom of the conduction band and the top of the valence band, respectively, and $\mathcal{F}_j(\eta)$ is the Fermi integral:

$$\mathcal{F}_j(\eta) = \frac{1}{\Gamma(j)} \int_0^\infty \frac{x^j dx}{\exp(x-\eta)+1}. \tag{10}$$

The value of η at each temperature can then be used to calculate $S(T)$ and $\sigma_s(T)$ for each band according to the expressions particular for the selected $\tau(T,E)$ dependence [39,44]:

$$S_C = \frac{k_B}{|e|}\left(-\eta + \frac{\mathcal{F}_1(\eta)}{\mathcal{F}_0(\eta)}\right), \tag{11}$$

$$S_V = \frac{k_B}{|e|}\left(\frac{\Delta}{T} + \eta\frac{\mathcal{F}_1(-\Delta/T-\eta)}{\mathcal{F}_0(-\Delta/T-\eta)}\right), \tag{12}$$

$$\sigma_C = e^2 \frac{8\pi}{3}\left(\frac{2}{h^2}\right)^{3/2} m_C^{1/2}\tau_{0c}\mathcal{F}_0(\eta) \equiv \sigma_{0C}\mathcal{F}_0(\eta), \quad (13)$$

$$\sigma_V = e^2 \frac{8\pi}{3}\left(\frac{2}{h^2}\right)^{3/2} m_V^{1/2}\tau_{0V}\mathcal{F}_0(-\Delta/T-\eta) \equiv \sigma_{0V}\mathcal{F}_0(-\Delta/T-\eta). \quad (14)$$

To clarify, the reduced Fermi level η is the Fermi level for electrons, $\eta \equiv \eta_c = (E_F - E_C)/k_BT$. The reduced Fermi level for holes, $\eta_v = (E_V - E_F)/k_BT$, is related to η as $\eta_v = -\Delta/T - \eta$.

Finally, total $\sigma_s(T)$ and $S(T)$ are calculated from

$$\sigma_s = \sigma_C + \sigma_V, \quad (15)$$

$$S = \frac{S_C\sigma_C + S_V\sigma_V}{\sigma_s}. \quad (16)$$

There are six parameters that determine $S(T)$ and $\sigma_s(T)$ according to Eqs. (8)–(16), namely gap value Δ, effective electron and hole masses m_C and m_V, density of doping carriers N_r, and temperature-independent prefactors for the conduction and valence band conductivity σ_{0C} and σ_{0V}. However, N_C, N_V, and N_r are linearly dependent in Eq. (8). Therefore we have selected the ratio $N_C/N_V = (m_C/m_V)^{3/2}$ and N_r, measured in units of N_V, as independent parameters together with Δ, σ_{0C}, and σ_{0V}.

The model also implies the condition N_r = constant, which corresponds to the independence of CDW wave vector q_1 from temperature [19]. This condition looks reasonable, in view of the absence of any signs of hysteresis in the $\sigma_s(T)$ curves.

We have varied the parameters to adjust the theoretical values to the experimental data of both $S(T)$ and $\sigma_s(T)$ concurrently. As we have shown in the previous section, close to T_{P1} the $\sigma_s(T)$ dependence is determined mainly by the PS process, so we expect the semiconductor model to work well in the temperature range sufficiently far from the CDW transition anomalies. Therefore we have used the experimental data of $\sigma_s(T)$ only in the temperature ranges between 200 K and 300 K, where good fits to the activated behavior have been obtained; see Fig. 3.

As for fitting $S(T)$, one can notice that the PS process affects strongly the S values near T_{P1} only in the high-Ohmic samples. On the other hand, in the low-Ohmic samples the effect of CDW-2 becomes strong below the isosbestic temperature $T_i \approx 225$ K, which might be attributed to the onset of the transition to the CDW-2 phase (see the discussion below). Therefore we have used experimental $S(T)$ data in the 200 K to 300 K range for the high-Ohmic samples and in the 250 K to 350 K range for the low-Ohmic samples. In these ranges S is roughly linear in T. Results of the fits are presented in Fig. 11.

The parameters of the fits are presented in Fig. 12. As N_C and N_V vary with temperature, see Eq. (9), while N_r does not, the N_r/N_V and N_r/N_C ratios are given for $T = 350$ K, slightly below T_{P1}. The m_C/m_V ratio is derived from the N_C/N_V ratio using Eq. (9). The τ_{0C}/τ_{0V} ratio is derived from σ_{0C}/σ_{0V} and m_C/m_V ratios using Eqs. (13) and (14).

For the most high-Ohmic sample, sample 8, we have obtained a good fit without involving doping, i.e., setting $N_r = 0$,

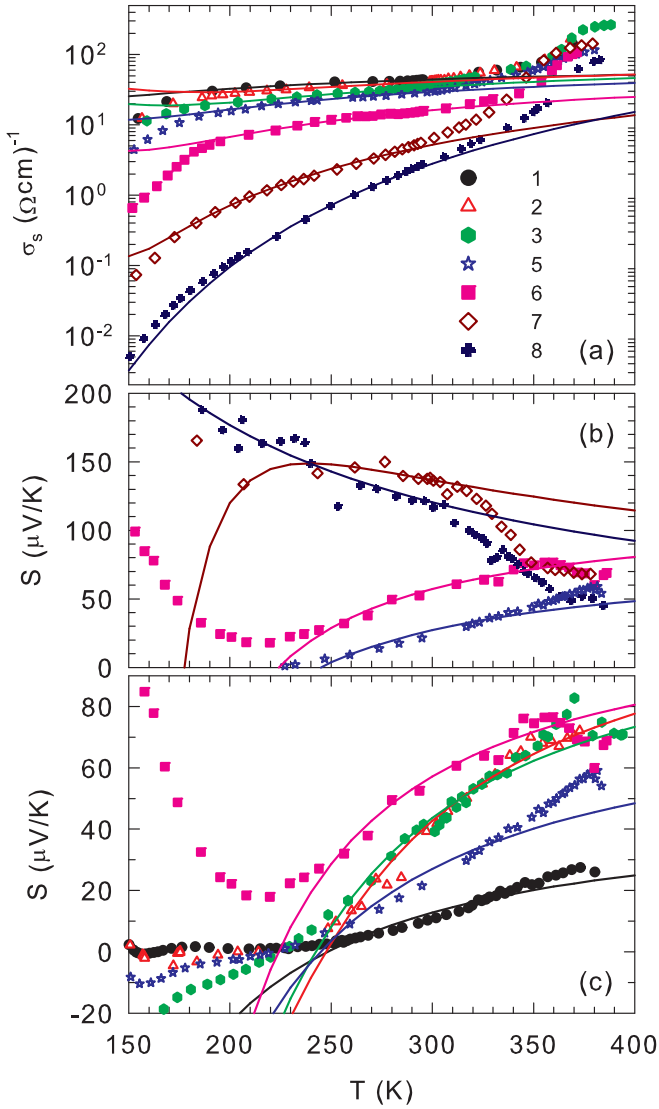

FIG. 11. Fit of $S(T)$ and $\sigma_s(T)$ between T_{P1} and T_{P2} using Eqs. (8)–(16). The fitting range for all $\sigma_s(T)$ curves and for $S(T)$ of high-Ohmic samples is 200 K to 300 K. For $S(T)$ of low-Ohmic samples it is 250 K to 350 K (see text). For each sample, the same parameters are used for the evaluation of both $S(T)$ and $\sigma_s(T)$.

and using the same value of τ_0, so that $\sigma_{0C} = \sigma_{0V}(m_C/m_V)^{1/2}$. Also, the gap $2\Delta \approx 4100$ K is close to the measured optical gap [16]. Therefore we suggest that sample 8 is an intrinsic CDW conductor in the temperature range between T_{P1} and T_{P2}. Finite positive S is due to the small difference in the effective masses of electrons and holes, $m_C/m_V \approx 1.5$, which would be expected for valence and conduction bands formed by the opening of the CDW gap [28]. The relaxation time τ_0, calculated assuming $m_C \approx m_e$, the free-electron mass, is $\tau_0 \approx 7 \times 10^{-14}$ s, which is a reasonable value for scattering by high-temperature phonons [45]. The fit also extrapolates well down to T_{P2}, indicating only small contribution of the CDW-2 phase.

For other samples we needed all five parameters to obtain reasonable fits. Even then the fits correspond well to the experimental data only in the fitting ranges and deviate strongly

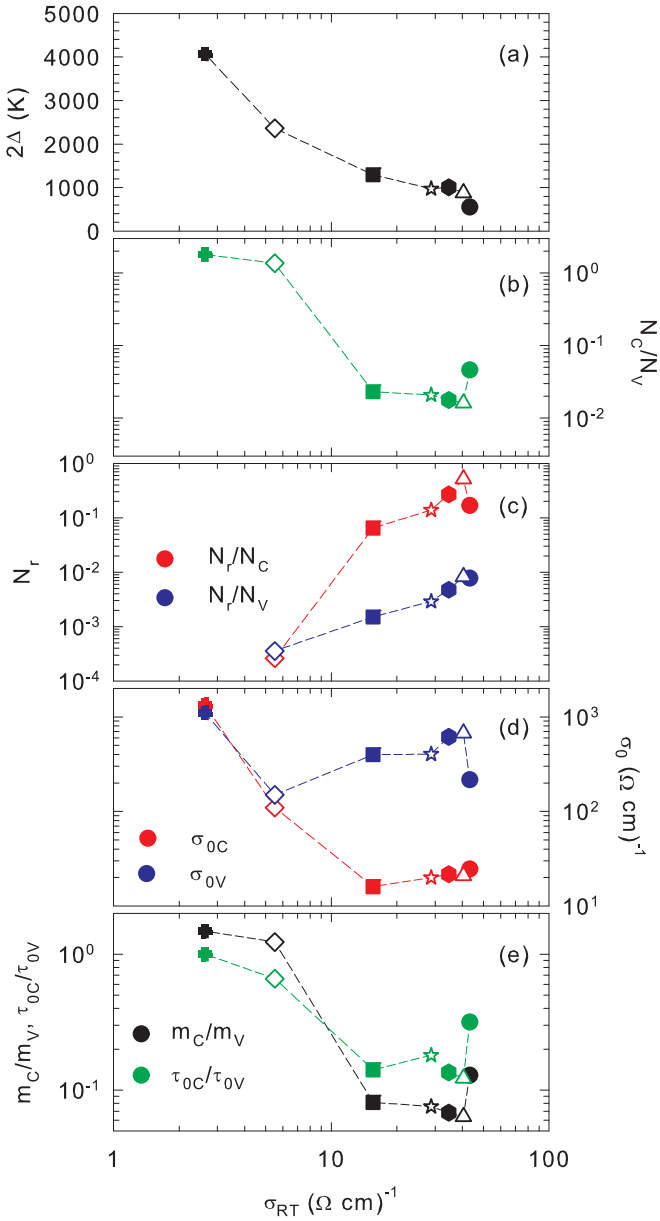

FIG. 12. Parameters for the fit of $S(T)$ and $\sigma_s(T)$ between T_{P1} and T_{P2} using Eqs. (8)–(16). Empty symbols are used for samples for which σ_{RT} has been only estimated. (a) Semiconducting gap Δ; (b) ratio of the effective densities of states in conduction and valence band N_C/N_V; (c) ratios of the (temperature independent) density of doping carriers N_r and the (temperature dependent) N_C and N_V at 350 K; (d) temperature-independent prefactors for the conduction and valence band conductivity σ_{0C} and σ_{0V}; (e) the ratio of the effective electron and hole masses, m_C/m_V, and the ratio of the carrier relaxation times, τ_{0C}/τ_{0V}, in the conduction and valence band.

at lower temperatures: the theoretical $\sigma_s(T)$ curves remain high, exceeding the experimental values, while the theoretical $S(T)$ curves drop below the experimental points, becoming negative. Finite, positive values of N_r indicate doping by electrons, Fig. 12(c), providing support to previous suggestion that sulfur vacancies behave as donors in sulfur-deficient samples [4].

The parameters for the other nominally high-Ohmic sample, sample 7, show some similarities with sample 8. The N_C/N_V ratio is nearly the same and σ_{0C} and σ_{0V} values are close to each other, as for sample 8. However, the gap is approximately two times smaller and small but finite N_r is required for a good fit. Also, absolute values of σ_{0C} and σ_{0V} are smaller than for sample 8, suggesting shorter relaxation times.

The good fits for low-Ohmic samples require quite high values of N_r, on the order of N_C, as shown in Fig. 12(c), so that the Fermi level is close to the conduction band, which gives the dominant contribution to $\sigma_s(T)$. Only much higher S_V due to negative hole Fermi level, see Eq. (8), keeps total S positive, at least until the saturation regime (in which the contribution of intrinsic thermally activated carriers becomes negligible) sets in at low temperature [46]. While the Fermi level close to the conduction band could account for the reduced E_{act} observed in the low-Ohmic samples [see Fig. 3(a)], the fits suggest that the gap is reduced as well, down to $2\Delta \approx 1000$ K, Fig. 12(a).

Moreover, in the low-Ohmic samples N_C and σ_{0C} are almost 2 orders of magnitude lower than N_V and σ_{0V}, while they are comparable in the high-Ohmic samples, Figs. 12(b) and 12(d). The m_C/m_V ratio, calculated from N_C/N_V and shown in Fig. 12(e), indicates that the effective electron mass in the conduction band is more than an order of magnitude lower that the effective hole mass in the valence band. Even taking into account the different effective masses, the relaxation time in low-Ohmic samples is almost an order of magnitude shorter for the conduction band than for the valence band, as the ratio of τ_{0C}/τ_{0V} in Fig. 12(e) shows.

Overall, $S(T)$ and $\sigma_s(T)$ curves of high-Ohmic samples between T_{P1} and T_{P2} are similar to those in intrinsic or lightly doped semiconductors, while in low-Ohmic samples they are typical of highly n-doped semiconductors.

We have tried to perform a similar fit to the semiconductor model for NbS_3-I sample 12, which shows a well-defined activation dependence of $\sigma_s(T)$. However, we did not find a combination of parameters that would give simultaneously the nearly linear temperature dependence of $S(T)$ and high E_{act} in $\sigma_s(T)$.

F. Specific heat of NbS_3-II

The experimentally obtained temperature dependence of the specific heat $c_p(T)$ is presented in Fig. 13. We have used the molar mass corresponding to the stoichiometric formula unit of NbS_3 to calculate the molar c_p. The $c_p(T)$ data show a distinct feature at T_{P1}, similar to those found for other compounds near the Peierls transitions [47,48], corroborating that the transition at T_{P1} is a usual Peierls transition. On the other hand, no features have been found around T_{P2}, highlighting the difference between the transitions at T_{P1} and T_{P2}.

Like in $K_{0.3}MoO_3$, TaS_3, and $(TaSe_4)_2I$, the feature at T_{P1} has a form of an asymmetric peak with the slope $|dc_p/dT|$ being higher to the right from the maximum of c_p than to the left. Thus, the $c_p(T)$ behavior around T_{P1} shows features of both a c_p jump, typical of second-order phase transitions, and a maximum revealing a distributed latent heat. Such a maximum has been suggested to be common for second-order

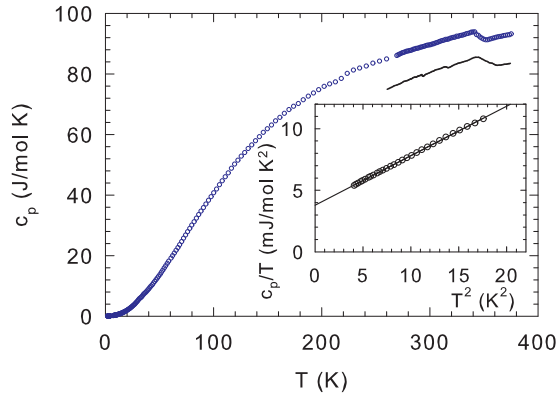

FIG. 13. The temperature dependence of the specific heat $c_p(T)$ of NbS_3-II. Solid line, shifted down by 10 J/(mol K), represents the estimate of c_p based on the PS model with the fraction **f** of the normal phase taken for high-Ohmic sample 7 shown in Fig. 9 (see text). The inset shows the analysis of low-temperature part of $c_p(T)$ revealing linear and cubic contributions.

phase transitions whose onset temperature is decreased by low-dimensional fluctuations [41,49]. For detailed analysis of the feature one should not forget that the data pictured in Fig. 13 result from averaging over a large number of whisker-like samples, whose properties are known to scatter.

Nevertheless, we have calculated the $c_p(T)$ dependence around T_{P1} expected from the PS model [41], $c_p(T) \sim d\mathbf{f}/dT$, using the numerically evaluated fraction **f** of the normal phase for the high-Ohmic sample 7 (Fig. 9). The derivative $d\mathbf{f}/dT$, multiplied by 300 and added to the baseline, is shown as the solid line in Fig. 13, shifted by 10 J/(mol K) down to avoid overlap. Except for the slightly shifted position of the maximum, there is strong similarity between the experimental $c_p(T)$ and the estimate based on PS model.

The low-temperature data are presented in the inset of Fig. 13 as c_p/T vs T^2, which clearly shows a linear and a cubic contribution, $c_p(T) = \gamma T + \beta T^3$. The cubic contribution is typical for acoustic phonons, as expected for crystalline materials, and the corresponding Debye temperature is $\theta_D = 270$ K. On the other hand, the linear contribution is typical for conducting electrons, which are not expected to be present in NbS_3-II at low temperatures, based on $\sigma_c(T)$ measurements. Moreover, the value of $\gamma = 3.78\,\mathrm{mJ/(mol\,K^2)}$ is comparable to γ values in metals.

IV. DISCUSSION

A. Thermopower of NbS_3-I

The semiconducting nature of NbS_3-I presumably comes from the gap in the half-filled lowest d band opened by dimerization of Nb atoms in the chains [31]. Band calculations [50] and XPS results [51] corroborate these assumptions. With the Fermi level positioned closer to the filled antibonding Nb band, as obtained from band calculations [52], the holes would be majority carriers and S would be positive. However, in ordinary semiconductors the value of $S(T)$ should increase and diverge as $1/T$ at low temperatures, while in NbS_3-I it slowly decreases.

A similar inconsistency (within the simple band theory) between the semiconducting decrease of $\sigma_s(T)$ and slow decrease of $S(T)$ at low temperatures has been observed in high-conductivity TCNQ complex salts [53]. The $S(T)$ dependence has been explained within the model of hopping conductivity of localized electrons with strong repulsion [53]. It is questionable whether the intrachain Nb-Nb dimerization can lead to the localization. Hall resistivity measurements could show whether the activated temperature dependence of conductivity comes from the decrease of the carrier density or from the decrease in mobility. Nevertheless, the constant $S = (k_B/e)\ln 2 \approx -60\ \mu\mathrm{V/K}$ seems to be a universal high-temperature limit in half-filled correlated electron systems with on-site repulsion [54,55], even in the presence of the gap at Fermi level [55]. The positive sign of S in NbS_3-I would require that the lowest electronic band, which is split by the dimerization, be of a holelike character, like the highest filled band in $TaSe_3$ [50]. Strong electron-electron correlations are also invoked to explain, at least qualitatively, the decrease of S at low temperatures in semiconducting phases of the high-T_c oxides [56,57] and full-Heusler compounds with pseudogaps [58,59].

B. Thermopower of NbS_3-II

1. High-temperature thermopower

Though $S(T)$ behavior in NbS_3-II samples correlates strongly with the room-temperature conductivity, i.e., with the doping level, at high temperatures $S(T)$ is very similar for all the samples (and close to the values for NbS_3-I), revealing p-type conductivity. The high-temperature conductivity values σ_{HT} are also fairly similar. Thus, both S and σ_s values are dominated by intrinsic carriers.

The two higher transitions at T_{P0} and T_{P1} can be associated with different CDW wave vectors [14]. The similarity of the structure and properties [12] to those of $NbSe_3$ and monoclinic TaS_3 [1,2] suggests that these CDWs modulate different chains and open gaps in different bands crossing the Fermi level [60]. Thus above T_{P1}, there is at least one partially filled band. In DFT calculations [4] performed on the simplified unit cell of NbS_3-II, i.e., the unit cell of NbS_3-I without the Nb-Nb dimerization, a flat band with two-thirds filling has been found. This can explain the CDW wave vector close to one-third (or, equivalently, two-thirds) and the positive, holelike value of S.

The constant value of S close to $(k_B/e)\ln 2$ measured in NbS_3 at high temperatures would be too high for an ordinary conduction band. However, in a simple model of the thermopower of a conductor with a bandwidth W comparable with T [61], S as a function of band filling n can be expressed as

$$S(T) = -\frac{k_B}{e}\ln\left(\frac{n}{1-n}\right). \tag{17}$$

With $n = 2/3$ obtained for NbS_3-II in DFT calculations [4], S would be exactly $(k_B/e)\ln 2$. Unfortunately, the condition $W \ll k_B T$ does not seem to be appropriate for NbS_3. Also, in this limit the electron (or hole) correlations play an important role [54,55].

Alternatively, such relatively high values can be found in metals with electrochemical potential [62] comparable with temperature (semimetals) [40] or in metals with a strong dependence of electron conductivity on energy originating, for

instance, from overlapping wide and narrow bands [63]. The first model would not be applicable for a one-third or two-thirds filled band, but there might be an overlap of the wide p band and narrow d band in NbS_3-II, as was suggested by the DFT calculations performed on the simplified unit cell [64].

2. Thermopower in the CDW-1 state

The $\sigma_s(T)$, $S(T)$, and $c_p(T)$ data around the transition at T_{P1} can be well described with a semiempirical model of spontaneous phase slippage [41], which confirms that the CDW-1 state is a typical Peierls state. However, below T_{P1} the temperature dependencies of S and σ_s become strongly sample dependent, presumably, due to the electron doping coupled with sulfur vacancies [4]. At the same time, T_{P1} does not vary substantially or systematically between samples. This suggests that the sample dependence does not come from the variation of electronic density in the chains in which the CDW-1 state develops, in agreement with the measurements of the Shapiro steps, i.e., the CDW synchronization by external high frequency field [11]. Moreover, photoconduction studies do not indicate the reduction of the CDW gap [16] either.

For the usual Peierls transition a change of electronic concentration would just result in a change of the CDW wave vector q, $\delta q = \pi \delta n$ (here n is the one-dimensional electronic concentration, i.e., concentration per CDW chain). This has been directly observed in V-doped $K_{0.3}MoO_3$ [65]. Although the conductivity and thermopower in this case have not been studied because of the poor quality of the V-doped samples [66], it is reasonable to assume that if the crystalline structure does not change, σ_s and S should not be very sensitive to the doping level.

The results of the modeling in Sec. III E indicate that the band structure responsible for the linear charge transport in NbS_3-II differs significantly between the high-Ohmic and low-Ohmic samples. The gap in low-Ohmic samples between valence and conduction band is reduced with respect to the high-Ohmic samples. The electrons and holes in high-Ohmic samples have similar effective masses and relaxation times, and the doping is small or negligible, as expected for the band structure of the CDW semiconductor [1,28]. On the other hand, in low-Ohmic samples electrons are much lighter than holes and relax much faster, i.e., scatter more often.

It is reasonable to suggest that the CDW band structure in the low-Ohmic samples is actually the same as in the high-Ohmic samples, but in the low-Ohmic samples another band near the Fermi level contributes to the charge transport as well. The electronic dispersions $E(k)$, where k is the electron wave vector, corresponding to the band structure in the high-Ohmic samples and to the two possible extended band structures for the low-Ohmic samples, are presented schematically in Fig. 14. The red and blue lines represent $E(k)$ in the conduction and the valence bands, respectively, and the black line the Fermi level in the low temperature saturation regime. Solid lines for $E(k)$ are based on the parameters of the fit, while the dashed lines represent possible extended band structures.

$E(k)$ presented in Fig. 14(b) corresponds to the band structure with a narrow band and, consequently, high effective mass of the holes, situated in the CDW gap near the conduction band, which effectively acts as the valence band. This resembles the impurity (or intermediate) bands formed in semiconductor materials by doping [67], or just by crystal defects (vacancies, interstitials) as in 2D transition metal chalcogenides [68]. However, these impurity bands are situated in the gap between electronic bands from different atomic orbitals while the CDW gap opens in the conduction band due to the lattice modulation [1]. It is not clear whether the sulfur vacancies in NbS_3-II would introduce in-gap states in the CDW gap as well.

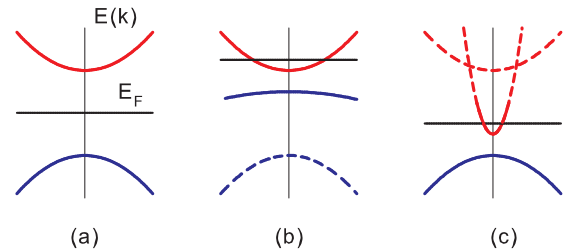

FIG. 14. Schematic electronic dispersions $E(k)$ for (a) high-Ohmic sample with simple CDW gap, (b) low-Ohmic sample with impurity band in CDW gap, and (c) low-Ohmic sample with electron pocket on the Fermi level.

Moreover, as the extra electrons from sulfur vacancies would originate from the impurity band, the Fermi level should be pinned to this band at low temperatures, while the model situates the Fermi level in the conduction band. Also, it would be reasonable to expect that relaxation time is shorter in the impurity band, while the model suggests the opposite. Finally, there would be optical transition between such impurity band and the conduction band, which is not observed in photoconduction studies [16].

$N(E)$ presented in Fig. 14(c) would correspond to the band structure with the electron pocket at the Fermi level with a low effective mass. Separate electron pockets on the edge of the Brillouin zone have been obtained in *ab initio* DFT calculations on a simplified NbS_3-II unit cell [4]. Opening of the CDW gap on the well-nested Fermi surfaces [2] would not involve the electronic states in these pockets. They can thus correspond to the in-gap conduction band with low density of conducting electrons below T_{P1}, as obtained from the semiconductor model of the low-Ohmic samples.

The mentioned DFT calculations have also shown that these pockets are very sensitive to doping, which might explain the difference between the high- and low-Ohmic samples. However, it is suggested that the pockets may eventually disappear in the case of excessive doping, so they would not contribute to the transport properties. This is exactly opposite to the suggestion that the sulfur vacancies are responsible for the properties of the low-Ohmic samples. Hopefully the calculation of the band structure in a realistic, more complex unit cell [12] will resolve this discrepancy and reveal more information about electronic bands contributing to the transport properties.

The electron pockets at the Fermi level can also develop in the case of imperfect nesting, as suggested for quasi-one-dimensional CDW systems [69] and extensively studied for quasi-two-dimensional CDW systems [70]. In order to account for the difference between the high- and low-Ohmic

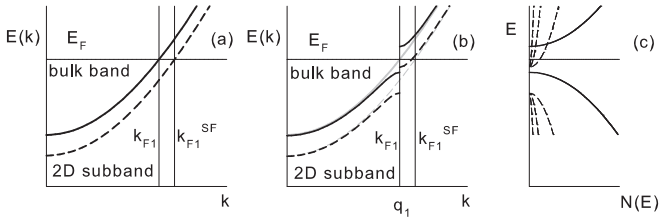

FIG. 15. (a) The electronic dispersions $E(k)$ in the bulk and 2D subband above T_{P1}. (b) The electronic dispersions in the bulk and 2D subband below T_{P1}, with CDW gap opened due to the q_1 modulation. (c) The density of states $N(E)$ in the bulk and 2D subband with different concentrations of SFs.

samples, the imperfect nesting in NbS_3-II should be induced by sulfur deficiency.

So far we have considered the NbS_3-II samples as homogeneous, with randomly distributed sulfur vacancies in low-Ohmic samples. However, STM studies of the surface of the low-Ohmic samples in the b_0-c_0 van der Waals plane [12,13,71] have revealed stacking faults (SFs), i.e., unit cells with extra Nb chains (e.g., 10 instead of 8 per cell). It has been shown that the SFs alter considerably the transport properties of different materials [72–74], which could also be relevant for NbS_3-II.

It has been suggested that the SFs act as quantum wells [72,75,76] with quasi-2D subband structure located in the SFs. In NbS_3-II the periodicity along the chains in the SFs is the same as in the bulk; thus it would be appropriate to suggest that the electron dispersion along the b axis is not altered, while the confinement along the c axis determines the energy of the bottom of the 2D subband in SFs with respect to equivalent band in the bulk. If the SF width is larger than that of the unit cell (5 interchain distances instead of 4), the 2D subband has slightly lower energy than the bulk band. Then the corresponding electron dispersions $E(k)$ along the chain, where k is the electron wave vector, would be as presented in Fig. 15(a), resembling the theoretical results for other compounds [77,78].

The periodic lattice distortion of $q_1 = 2k_{F1}$, which accompanies CDW formation, leads to the opening of the gap at the Fermi wave vector k_{F1} in the bulk band. The CDW coherence persists over several unit cells even in highly doped samples of the structurally similar system $NbSe_3$ [79]. Therefore, the periodic distortion should affect the SF band structure as well, opening the gap in the 2D subband at the same wave vector k_{F1}. However, the Fermi wave vector k_F^{SF} in the 2D subband is slightly larger than in the bulk, as presented in Fig. 15(b), so the gap opens below E_F in the 2D subband. Thus, below T_{P1} the overgap states of the subband will make a sort of conducting band with low density of states, populated with electrons.

Such model qualitatively conforms to all results of the modeling in Sec. III E, particularly to the extended band structure presented in Fig. 15(c). First, the gap between these new valence and conduction bands would be smaller than the CDW gap. Second, $N(E)$ in the conduction band [Fig. 15(c)], which arises from the 2D subband confined to the SF, would be proportional to the volume fraction of SFs, that is, much lower than $N(E)$ in the bulk valence band. Third, the electron-hole balance is naturally disrupted as some extra electrons remain in the conduction band below T_{P1}, and the density of such "doping" electrons N_r would be proportional to $N(E)$ in the conduction band. Finally, the relaxation time of electrons in the 2D subband is expected to be lower than in the bulk band [72].

3. Isosbestic point T_i

The convergence of the $S(T)$ curves at $T_i \approx 225$ K [Fig. 1(c)] deserves a special discussion. While such intersections of curves with a varying parameter have been observed for different physical quantities, no universal explanation of the origin of these isosbestic points has been suggested [34]. In the case of NbS_3-II, the $\sigma_s(T)$ curves do not show any features around T_i [Fig. 1(a)]. Therefore, T_i is not likely to be the point of a phase transition. The close-to-zero value of S could indicate a compensation of the electron and hole contributions at T_i. Taking into account that at T_i thermopower is nearly independent of the concentration of the doping-induced electrons, one can further conclude that their contribution to S is close to zero, as well as the contribution of the holes from the main band.

The sign change of S in NbS_3-II can happen above a CDW transition due to 1D fluctuations, as has been reported for $K_{0.3}MoO_3$ [80]. In this case the zero value of S corresponds to the mutual compensation of the metallic and CDW contributions. In terms of the electron-energy dispersion curve, $E(k)$, the CDW-2 fluctuations do not yet result in a gap, but affect the curvature of the $E(k)$ line at the Fermi energy, making its effective value close to zero. If this is the case, a small change of electronic concentration will not result in a significant change of S. A wide region of fluctuations around T_{P2}, interpreted as a freezing of the electronic density distortion (ordering) with cooling, has been revealed by the NMR technique [4]. This result supports the relation of T_i in NbS_3-II with 1D fluctuations. Thus, the fluctuation origin of the isosbestic point [Fig. 1(c)] seems reasonable.

4. Thermopower and the condensation of doping-induced electrons at T_{P2}

The transition at T_{P2} is clearly observed only in the low-Ohmic samples, as the steplike decrease of $\sigma_s(T)$ and the steplike increase of $S(T)$. Such evolution is characteristic of semiconducting CDW transitions [23–27]. In the high-Ohmic samples it can be seen near T_{P1}. As we have shown, the dominant contribution to σ_s of the low-Ohmic samples at $T_{P2} < T < T_{P1}$ comes from electron doping, which is also responsible for the S decrease. Previous studies have shown that the charge density condensed in CDW-2 is extremely low and sample dependent [4,11], being proportional to the conductivity above T_{P2} [4]. Thus our results support the suggestion [4] that the CDW-like transition at T_{P2} corresponds to the dielectrization of these doping-induced electrons. Per contra, the high-Ohmic samples, with small or negligible doping, show only slight increase of slope in $\sigma_s(T)$ and slightly faster increase of $S(T)$ below T_{P2}.

Despite the strong sample dependence of the transport properties of NbS_3-II, especially of $S(T)$, below T_{P1}, as well as around and below T_{P2}, the transition temperature T_{P2} is very stable against variations in σ_{RT}, and for the majority of the

samples it is close to 150 K [Fig. 4(b)] [4,5]. This might be expected if T_{P2} signifies the CDW transition in the 2D subband in SFs (Fig. 15). As the local atomic arrangement within a SF is well defined [12,13,71], T_{P2} should be the same regardless on the number of SFs in the sample.

At the same time, $T_{P2} = 150$ K is likely to be a marked point for the high-Ohmic samples as well. Presumably, one can find indications of the transition in their conductivity as well, though not quite straightforward. A feature near 150 K was detected in $\sigma(T)$ of NbS_3 samples measured at high frequencies [9], while in the dc measurements the conductivity was falling smoothly with activation energy ~1300 K, akin to our high-Ohmic phase-II samples. Though we did not perform high-frequency studies on our samples, we took into account that in the CDW systems the dependencies of conductivity on frequency and on voltage can look similar [81,82]. Studying I-V curves of the high-Ohmic samples we found that in the region of T_{P2} they show an onset of gradual nonlinear conductivity, known also as threshold rounding [83]. It is notable that even in NbS_3-I a feature near 150 K in $\sigma(T)$ appears under pressure [84].

These results suggest that the mechanism of the transition at T_{P2} is intrinsic to NbS_3; i.e., it does not depend on the density of electrons condensed in the CDW-2 state, which can vary by several orders of magnitude. Within the theory of the Peierls transition [85,86] different band filling should affect the transition temperature. Thus it was proposed [4,11] that the CDW-2 state might be an excitonic insulator [87,88], where the transition temperature is determined only by the exciton binding energy [89]. Such state can occur when there is a small gap between electron and hole pockets in the Brillouin zone, which we already considered in Sec. IV B 2 as a possible explanation of transport properties of the low-Ohmic samples in the CDW-1 phase.

Below T_{P2}, $\sigma_s(T)$ of the low-Ohmic samples seems to resume the activated behavior [4]. Activation energy E_{act}, estimated in the limited temperature range, is around $E_{act} =$ 1000 K, about half of E_{act} in the high-Ohmic samples. However, only several low-Ohmic samples with lower σ_{RT} show $S(T)$ increasing at lower temperatures, as expected for the semiconducting regime, approaching the S values of the high-Ohmic samples. For most low-Ohmic samples $S(T)$ remains very low, saturating at values of about 10 μV/K, more appropriate for metallic systems. Only in sample 3 [35] E_{act} below T_{P2} remains as small as above, as in several previously studied samples [5]. This is reflected in $S(T)$, which does not show any feature at T_{P2} and decreases to highly negative values at low temperatures, suggesting there remain extra electrons in this sample even below T_{P2}. Such variation of $S(T)$ dependencies between the samples confirms that in the semiconducting regime $S(T)$ is much more sensitive to the details of the doping from localized impurities and the corresponding electron-hole balance than $\sigma_s(T)$; compare, e.g., [90,91]. For instance, samples 3 and (maybe) 11 could contain electrons from some point defects that are not gapped by any of the transitions.

C. Specific heat of NbS_3-II near and below T_{P2}

We have shown in Sec. III F that the asymmetric peak in specific heat $c_p(T)$ of NbS_3-II at T_{P1} is typical for the Peierls transition [47,48]. The transition at T_{P2}, however, cannot be detected in $c_p(T)$. The experimentally evidenced opening of the gap should manifest itself, at least, as the mean-field jump in $c_p(T)$, in the case of the excitonic insulator formation [92], or a more pronounced feature in the case of the CDW transition with strong fluctuations [47,49]. However, if the density of electrons affected by the CDW-2 transition is much lower than for the CDW-1 transition, as we have discussed in the previous section, then their contribution to $c_p(T)$ might be too low to notice on top of the dominant phonon contribution.

At low temperatures $c_p(T)$ features a free-electron-like linear contribution that is not expected in fully dielectric NbS_3-II at low temperatures. A quasilinear contribution of low-energy excitations (LEEs) to $c_p(T)$ has been observed in many semiconducting CDW systems [93]; however it shows only below about 1 K, as its amplitude is at least an order of magnitude lower than in NbS_3-II. Comparison of the Curie-like magnetic susceptibility $\chi(T)$ and $c_p(T)$ suggests that LEEs correspond to $s = 1/2$ spins localized at random lattice sites [94]. Incidentally, spinon excitations in Heisenberg $s = 1/2$ spin chains also give a large linear contribution to $c_p(T)$ [95], but with quite distinctive $\chi(T)$ [96]. Thus $\chi(T)$ measurements of NbS_3-II might help to resolve the origin of the linear term.

V. CONCLUSION

We have studied the temperature dependence of the Seebeck effect $S(T)$ in different NbS_3 samples in a wide temperature range together with their temperature-dependent conductivity $\sigma_s(T)$. For all the samples S at high temperature is positive, on the order of k_B/e, and weakly depends on temperature. The studies of NbS_3-II samples have revealed the features at both T_{P1} and T_{P2} transitions; however below T_{P1}, and particularly below T_{P2}, $S(T)$ dependence is strongly sample dependent. In NbS_3-I samples $S(T)$ decreases almost linearly with temperature decrease despite the semiconducting nature of $\sigma_s(T)$, suggesting either a hopping mechanism of conductivity or the influence of strong electronic correlations.

Our results for phase II clearly show that below T_{P1} the $S(T)$ curves vary rather systematically as a function of the room-temperature conductivity σ_{RT}. Between T_{P1} and T_{P2}, i.e., in the CDW-1 state, we have simultaneously parametrized $S(T)$ and $\sigma_s(T)$ using a simple semiconductor model. The results demonstrate that the high-Ohmic samples are intrinsic CDW semiconductors, while in the low-Ohmic samples the transport properties are dominated by a band with low density of states and itinerant electrons. The band is situated within the CDW gap and can either correspond to separate pocket bands at the Fermi surface, intrinsic to NbS_3-II, or originate from the bands localized within the stacking faults. In each case, we suggest an appropriate theoretical model for the transition to the CDW-2 state.

For readers' convenience, we summarize the results of our paper in the following list:

(1) The temperature dependence of the electric conductivity $\sigma_s(T)$ and Seebeck coefficient $S(T)$ has been measured in a wide temperature range (100 K to 400 K) on multiple samples of the quasi-one-dimensional conductor NbS_3, including both type-I and type-II phases and both low-Ohmic and high-Ohmic subphases of NbS_3-II.

(2) At high temperatures $S(T)$ for all samples is positive and on the order of k_B/e.

(3) $S(T)$ of NbS_3-I samples decreases as temperature is lowered, while $\sigma_s(T)$ increases in the activated manner. These features put phase I beyond the family of classical semiconductors and might be explained by strong electron-electron correlations.

(4) Both $\sigma_s(T)$ and $S(T)$ evolve gradually between high- and low-Ohmic samples of NbS_3-II. At the same time, CDW transition temperatures T_{P1} and T_{P2} do not vary substantially and systematically between the samples.

(5) Characteristics of the low-Ohmic NbS_3-II samples [with $\sigma_{RT} \gtrsim 10\ (\Omega\ \mathrm{cm})^{-1}$] are the gradual decrease of $S(T)$ below T_{P1} and steplike decrease of $\sigma_s(T)$ at T_{P2}. The features in $S(T)$ at T_{P1} confirm (partial) gapping of the remaining free electrons.

(6) The $S(T)$ curves of the low-Ohmic samples converge at $T_i \approx 225$ K, where their values appear close to zero. The convergence could be explained by the onset of CDW-2 fluctuations, which make the quasiparticles cross over from metallic to dielectric behavior around T_i.

(7) The thermopower of the high-Ohmic NbS_3-II samples [with $\sigma_{RT} < 10\ (\Omega\ \mathrm{cm})^{-1}$] shows a step at T_{P1} and further growth with T decrease. The $\sigma_s(T)$, $S(T)$, and $c_p(T)$ curves around T_{P1} can be described in terms of the growth of the fraction of the normal phase with T approaching T_{P1}. Their T dependencies agree with the semiempirical model of spontaneous phase slippage.

(8) We have successfully modeled the $S(T)$ and $\sigma_s(T)$ dependencies between T_{P1} and T_{P2} using a narrow-gap semiconductor model with doping. The model parameters demonstrate that the high-Ohmic samples are intrinsic CDW semiconductors with low level of doping, while in the low-Ohmic samples the transport properties are dominated by a conduction band with a low density of states.

(9) We show that the 2D subbands coupled with the stacking faults, previously observed in NbS_3-II samples, can qualitatively account for the properties of low-Ohmic NbS_3-II samples.

We also should mention several unsolved problems.

(1) The origin of the band with low density of states within the gap of NbS_3-II is still dubious. It could be an electronic pocket intrinsic to the basic structure of NbS_3-II, but it could be related to stacking faults or some other structural defects of this compound. It is still not clear whether the stacking faults are related to sulfur shortage.

(2) The origin of the transition at T_{P2} is not clear. Some experimental results argue for the relation of the transition to stacking faults; some others argue for the volume transition, such as condensation of a narrow-band semiconductor into an excitonic insulator.

(3) There is at least one extra parameter affecting NbS_3-II transport properties. Samples with lower conductivity can show higher conductivity below T_{P2}. We can only assume that these samples contain electrons from point defects that are not gapped by any of the transitions.

(4) Though the S behavior of NbS_3-I samples clearly excludes them from the family of classical semiconductors, further classification of this isomer is only guessable.

ACKNOWLEDGMENTS

We are grateful to A. A. Sinchenko and A. Prodan for useful discussions. The work was supported by RFBR (Grants No. 16-02-01095, No. 17-02-01343, and No. 17-02-00211) and the programs of the Russian Academy of Sciences and Slovenian-Russian Project No. ARRS-MS-BI-RU-JR-Prijava/2016/51. The techniques of thermopower studies and the analyses of the *R-S* scaling were elaborated in the framework of RSF Grant No. 17-12-01519. V.F. Nasretdinova performed synthesis of NbS_3 crystals in the framework of the Russian State task. A.N. and O.S. acknowledge the Ministry of Education and Science of the Russian Federation in the framework of Increase Competitiveness Program of NUST "MISiS" Grant No. K2-2017-084, by Acts 211 of the Government of the Russian Federation, Contracts No. 02.A03.21.0004, No. 02.A03.21.0006, and No. 02.A03.21.0011. W.W.P. is supported by MOST, Taiwan (Grant No. 107-2112-M-002-017-MY3) and by the AI-MAT Center of National Taiwan University (Grant No. NTU-107L900802). D.S. acknowledges financial support by the Center of Excellence for Advanced Materials and Sensors established by the Ministry of Science and Education of the Republic of Croatia.

[1] P. Monceau, in *Electronic Properties of Inorganic Quasi-One-Dimensional Conductors*, edited by P. Monceau (D. Reidel Publishing Company, Dordrecht, 1985), p. 2.

[2] P. Monceau, Adv. Phys. **61**, 325 (2012).

[3] M. A. Bloodgood, P. Wei, E. Aytan, K. N. Bozhilov, A. A. Balandin, and T. T. Salguero, APL Mater. **6**, 026602 (2018).

[4] S. G. Zybtsev, V. Ya. Pokrovskii, V. F. Nasretdinova, S. V. Zaitsev-Zotov, V. V. Pavlovskiy, A. B. Odobesco, Woei Wu Pai, M.-W. Chu, Y. G. Lin, E. Zupanič, H. J. P. van Midden, S. Šturm, E. Tchernychova, A. Prodan, J. C. Bennett, I. R. Mukhamedshin, O. V. Chernysheva, A. P. Menushenkov, V. B. Loginov, B. A. Loginov, A. N. Titov, and Mahmoud Abdel-Hafiez, Phys. Rev. B **95**, 035110 (2017).

[5] S. G. Zybtsev, V. Ya. Pokrovskii, V. F. Nasretdinova, and S. V. Zaitsev-Zotov, Appl. Phys. Lett. **94**, 152112 (2009).

[6] In [4,7] the value $T_{P0} \sim 600$ K has been reported. However, due to the degradation of the chromel-alumel thermocouple, the temperatures above ~400 K were substantially overestimated. Roughly, in °C they were 1.6–1.7 above the actual value.

[7] S. G. Zybtsev, V. Ya. Pokrovskii, V. F. Nasretdinova, and S. V. Zaitsev-Zotov, The anomalous features of the CDWs in the monoclinic phase of NbS_3, in *International School and Workshop on Electronic Crystals ECRYS-2017, August 21–September 2, 2017* (Cargese, France, 2017).

[8] V. Ya. Pokrovskii, S. G. Zybtsev, M. V. Nikitin, I. G. Gorlova, V. F. Nasretdinova, and S. V. Zaitsev-Zotov, Usp. Fiz. Nauk **183**, 33 (2013) [Phys. Usp. **56**, 29 (2013)].

[9] M. Izumi, T. Nakayama, R. Yoshizaki, K. Uchinokura, T. Iwazumi, T. Seino, and E. Matsuura, in *Proceedings of the*

International Symposium on Nonlinear Transport and Related Phenomena in Inorganic Quasi-One-Dimensional Conductors (Hokkaido University, Sapporo, 1983), p. 301.
[10] B. Fisher and M. Fibich, Solid State Commun. **59**, 187 (1986).
[11] S. G. Zybtsev, V. Ya. Pokrovskii, V. F. Nasretdinova, and S. V. Zaitsev-Zotov, Phys. B (Amsterdam) **407**, 1696 (2012).
[12] E. Zupanič, H. J. P. van Midden, M. A. van Midden, S. Šturm, E. Tchernychova, V. Ya. Pokrovskii, S. G. Zybtsev, V. F. Nasretdinova, S. V. Zaitsev-Zotov, W. T. Chen, Woei Wu Pai, J. C. Bennett, and A. Prodan, Phys. Rev. B **98**, 174113 (2018).
[13] Woei Wu Pai, M. W. Chu, W. T. Chen, V. Ya. Pokrovskii, S. V. Zaitsev-Zotov, S. G. Zybtsev, V. F. Nasretdinova, M. D. Ustenko, E. Zupanič, H. J. P. van Midden, M. van Midden, S. Ŝturm, A. Prodan, E. Tchernychova, and J. C. Bennett, in *Proceedings of the XXII International Symposium "Nanophysics and Nanoelectronics"* (Publishing House of N. I. Lobachevsky Nizhny Novgorod State University, Nizhny Novgorod, 2018), Vol. 1, p. 285.
[14] Z. Z. Wang, P. Monceau, H. Salva, C. Roukau, L. Guemas, and A. Meerschaut, Phys. Rev. B **40**, 11589 (1989).
[15] At the same time, the composition cannot be responsible for all the variety of NbS_3-II properties. Some samples show an additional transition around 300–340 K (see, e.g., [5]), which in some cases looks like a broadening of the T_{P1} transition. Also, samples are found which below 620 K show only the T_{P2} transition or no transitions at all [13]. The form of the $\sigma_s(T)$ curves, especially near T_{P1} and T_{P2}, can vary for samples with the same value of σ_s(290 K). Presumably, the defect (stacking-fault) structure strongly affects the specific conductivity of NbS_3-II and the CDW transitions in it. See also [3].
[16] V. Nasretdinova, V. Pokrovsky, S. V. Zaitsev-Zotov, and S. G. Zybtsev, Light-induced transition from hard to soft gap in CDW conductor NbS_3(phase II) at 77 K, in Nonequilibrium Phenomena in Complex Matter: New Observations and New Theories, Ambrož, Krvavec, Slovenia, 13–16 December 2015, Book of Abstracts, pp. 46–47, http://f7-4.ijs.si/db_images/Abstract%20book%20Krvavec%202015-final.pdf.
[17] F. W. Boswell and A. Prodan, Physica (Amsterdam) **99B**, 361 (1980).
[18] C. Roucau, J. Phys. (Paris) Coll. **44**, C3–1725 (1983).
[19] M. E. Itkis, F. Ya. Nad', S. V. Zaitsev-Zotov, and F. Levy, Solid State Commun. **71**, 895 (1989).
[20] M. E. Itkis, F. Ya. Nad', and F. Levy, Synth. Metals **41–43**, 3969 (1991).
[21] V. Nasretdinova and S. V. Zaitsev-Zotov, Physica B (Amsterdam) **407**, 1874 (2012).
[22] P. M. Chaikin, in *Organic Superconductivity*, edited by V. Z. Kresin and W. A. Little (Plenum Press, New York, 1990), p. 101.
[23] B. Fisher, Solid State Commun. **46**, 227 (1983).
[24] D.-L. Zhang, S.-Y. Lin, B. J. Lin, and C. W. Chu, Phys. Rev. B **37**, 4502 (1988).
[25] K. Surendranath, C. Bansal, and A. Meerschaut, Solid State Commun. **60**, 173 (1986).
[26] A. Smontara, K. Biljaković, J. Mazuer, P. Monceau, and F. Levy, J. Phys.: Condens. Matter **4**, 3273 (1992).
[27] D. Starešinić, M. Očko, K. Biljaković, and D. Dominko, arXiv:1408.6190.
[28] S. N. Artemenko, V. Ya. Pokrovskii, and S. V. Zaitsev-Zotov, Zh. Eksp. Teor. Fiz. **110**, 1069 (1996) [JETP **83**, 590 (1996)].
[29] S. G. Zybtsev *et al.* (unpublished).
[30] C. Schlenker, J. Dumas, C. Escribe-Filippini, H. Guyot, J. Marcus, and G. Fourcaudot, Philos. Mag. B **52**, 643 (1985).
[31] J. Rijnsdorp and F. Jellinek, J. Solid State Chem. **25**, 325 (1978).
[32] E. Finkman and B. Fisher, Solid State Commun. **50**, 25 (1984).
[33] E. Slot, M. A. Holst, H. S. J. van der Zant, and S. V. Zaitsev-Zotov, Phys. Rev. Lett. **93**, 176602 (2004).
[34] M. Greger, M. Kollar, and D. Vollhardt, Phys. Rev. B **87**, 195140 (2013).
[35] For this sample σ_s(290 K) is 34 $(\Omega\,\mathrm{cm})^{-1}$, which is not the highest value [4]. The transition at 150 K is smeared out, and the dielectrization of the electronic spectrum below 150 K is incomplete. This sample is suggested to be defective, probably, impure or not single phase.
[36] Z. X. Dai, C. G. Slough, and R. V. Coleman, Phys. Rev. B **45**, 9469 (1992).
[37] S. G. Zybtsev, V. Ya. Pokrovskii, and S. V. Zaitsev-Zotov, Nat. Commun. **1**, 85 (2010).
[38] D. Dominko and D. Starešinić, J. Phys.: Condens. Matter **22**, 055603 (2010).
[39] K. Seeger, *Semiconductor Physics* (Springer-Verlag, Berlin, 2004), p. 81.
[40] T. Okuda, K. Nakanishi, S. Miyasaka, and Y. Tokura, Phys. Rev. B **63**, 113104 (2001).
[41] V. Ya. Pokrovskii, A. V. Golovnya, and S. V. Zaitsev-Zotov, Phys. Rev. B **70**, 113106 (2004).
[42] S. G. Zybtsev, V. Ya. Pokrovskii, O. M. Zhigalina, D. N. Khmelenin, D. Starešinić, S. Šturm, and E. Tchernychova, JETP **124**, 665 (2017).
[43] Y. Apertet, H. Ouerdane, C. Goupil, and Ph. Lecoeur, Energy Conversion and Management **93**, 160 (2015).
[44] H. J. Goldsmid, *Introduction to Thermoelectricity* (Springer-Verlag, Berlin, 2010), p. 23.
[45] C. Jacoboni, *Theory of Electron Transport in Semiconductors* (Springer-Verlag, Berlin, 2010), p. 201.
[46] J. S. Blakemore, *Semiconductor Statistics* (Pergamon Press, Oxford, 1962), p. 106.
[47] R. S. Kwok, G. Gruner, and S. E. Brown, Phys. Rev. Lett. **65**, 365 (1990).
[48] D. Starešinić, A. Kiš, K. Biljaković, B. Emerling, J. W. Brill, J. Souletie, H. Berger, and F. Lévy, Eur. Phys. J. B **29**, 71 (2002).
[49] V. Ya. Pokrovskii, J. Phys. IV (France) **131**, 315 (2005).
[50] D. W. Bullett, J. Phys. C: Solid State Phys. **12**, 277 (1979).
[51] K. Endo, H. Ihara, K. Watanabe, and Shun-Ichi Gonda, J. Solid State Chem. **39**, 215 (1981).
[52] D. W. Bullett, J. Solid State Chem. **33**, 13 (1980).
[53] I. F. Shchegolev, Phys. Status Solidi A **12**, 9 (1972).
[54] P. M. Chaikin and G. Beni, Phys. Rev. B **13**, 647 (1976).
[55] E. M. Conwell, Phys. Rev. B **18**, 1818 (1978).
[56] J. B. Mandal, S. Keshri, P. Mandal, A. Poddar, A. N. Das, and B. Ghosh, Phys. Rev. B **46**, 11840 (1992).
[57] V. Ponnambalam and U. V. Varadaraju, Phys. Rev. B **52**, 16213 (1995).
[58] Dat Do, M.-S. Lee, and S. D. Mahanti, Phys. Rev. B **84**, 125104 (2011).
[59] Y. Nishino, H. Kato, M. Kato, and U. Mizutani, Phys. Rev. B **63**, 233303 (2001).
[60] E. Canadell, I. E.-I. Rachidi, J. P. Pouget, P. Gressier, A. Meerschaut, J. Rouxel, D. Jung, M. Evain, and M.-H. Whangbo, Inorg. Chem. **29**, 1401 (1990).

[61] B. Fisher and M. Fibich, Phys. Rev. B **37**, 2820 (1988).
[62] Y. Apertet, H. Ouerdane, C. Goupil, and Ph. Lecoeur, Eur. Phys. J. Plus **131**, 76 (2016).
[63] T. Takeuchi, Materials Transactions **50**, 2359 (2009).
[64] A. N. Enyashin and A. L. Ivanovskii, Phys. Solid State **48**, 780 (2006).
[65] S. Ravy, S. Rouzière, J.-P. Pouget, S. Brazovskii, J. Marcus, J.-F. Bérar, and E. Elkaim, Phys. Rev. B **74**, 174102 (2006).
[66] S. Ravy (private communication).
[67] A. Dashora, N. Patel, D. C. Kothari, B. L. Ahuja, and A. Miotello, Sol. Energy Mater. Sol. Cells **125**, 120 (2014).
[68] A. V. Krivosheeva, V. L. Shaposhnikov, V. E. Borisenko, J.-L. Lazzari, C. Waileong, J. Gusakova, and B. K. Tay, J. Semicond. **36**, 122002 (2015).
[69] G. Mihaly, A. Virosztek, and G. Gruner, Phys. Rev. B **55**, R13456 (1997).
[70] V. Brouet, W. L. Yang, X. J. Zhou, Z. Hussain, R. G. Moore, R. He, D. H. Lu, Z. X. Shen, J. Laverock, S. B. Dugdale, N. Ru, and I. R. Fisher, Phys. Rev. B **77**, 235104 (2008).
[71] Woei Wu Pai *et al.* (unpublished).
[72] A. Segura, B. Mari, J. Martinez-Pastor, and A. Chevy, Phys. Rev. B **43**, 4953 (1991).
[73] F. Fabbri and A. Cavallini, J. Appl. Phys. **108**, 013702 (2010).
[74] E. Koren, A. W. Knoll, E. Lörtscher, and U. Duerig, Nat. Commun. **5**, 5837 (2014).
[75] Y. T. Rebane, Y. G. Shreter, and M. Albrecht, Phys. Status Solidi A **164**, 141 (1997).
[76] H. Iwata, U. Lindefelt, S. Öberg, and P. R. Briddon, Phys. Rev. B **65**, 033203 (2001).
[77] U. Lindefelt, H. Iwata, S. Öberg, and P. R. Briddon, Phys. Rev. B **67**, 155204 (2003).
[78] A. Belabbes, L. C. de Carvalho, A. Schleife, and F. Bechstedt, Phys. Rev. B **84**, 125108 (2011).
[79] S. Rouziere, S. Ravy, J.-P. Pouget, and R. E. Thorne, Phys. Rev. B **59**, 15121 (1999).
[80] A. Janossy, G. Mihaly, S. Pekker, and S. Roth, Solid State Commun. **61**, 33 (1987).
[81] G. Grüner, A. Zettl, W. G. Clark, and J. Bardeen, Phys. Rev. B **24**, 7247 (1981).
[82] D. Starešinić, K. Biljaković, W. Brütting, K. Hosseini, P. Monceau, H. Berger, and F. Levy, Phys. Rev. B **65**, 165109 (2002).
[83] S. G. Zybtsev *et al.* (unpublished).
[84] E. M. Dizhur, M. A. Il'ina, and S. V. Zaitsev-Zotov, JETP Lett. **86**, 132 (2007).
[85] M. J. Rice and S. Strässler, Solid State Commun. **13**, 125 (1973).
[86] D. Allender, J. W. Bray, and J. Bardeen, Phys. Rev. B **9**, 119 (1974).
[87] L. V. Keldysh and Yu. V. Kopaev, Fiz. Tverd. Tela **6**, 2791 (1964) [Sov. Phys. Solid State **6**, 2219 (1965)].
[88] W. Kohn, Phys. Rev. Lett. **19**, 439 (1967).
[89] A. N. Kozlov and L. A. Maksimov, Zh. Eksp. Teor. Fiz. **48**, 1184 (1965) [Sov. Phys. JETP **21**, 790 (1965)].
[90] T. H. Geballe and G. W. Hull, Phys. Rev. **98**, 940 (1954).
[91] P. J. Morin and J. P. Maita, Phys. Rev. **96**, 28 (1954).
[92] K. Sugimoto, T. Kaneko, and Y. Ohta, Phys. Rev. B **93**, 041105(R) (2016).
[93] K. Biljaković, D. Starešinić, D. Dominko, and J. C. Lasjaunias, Phys. B (Amsterdam) **404**, 456 (2009).
[94] K. Biljaković, M. Miljak, D. Starečinić, J. C. Lasjaunias, P. Monceau, H. Berger, and F. Levy, Europhys. Lett. **62**, 554 (2003).
[95] A. V. Sologubenko, E. Felder, K. Gianno, H. R. Ott, A. Vietkine, and A. Revcolevschi, Phys. Rev. B **62**, R6108 (2000).
[96] N. Motoyama, H. Eisaki, and S. Uchida, Phys. Rev. Lett. **76**, 3212 (1996).